Université de Montréal

The effects of oxidative stress on the retinal structure and function

Par
Mikheil Djavari

Département de pharmacologie
Faculté de médecine

Mémoire présenté à la Faculté des études supérieures
En vue de l'obtention du grade de Maître ès sciences (M.Sc.)
en pharmacologie

Octobre 2010

Université de Montréal
Faculté des études supérieures et postdoctorales

Ce mémoire intitulé :
The effects of oxidative stress on the retinal structure and function

présenté par :
Mikheil DJAVARI

a été évalué par un jury composé des personnes suivantes :

Dr Denis DeBlois
président-rapporteur

Dr Sylvain Chemtob
directeur de recherche

Dr Pierre Lachapelle
codirecteur de recherche

Dr Gilbert Blaise
membre du jury

Résumé

Des études antérieures ont démontré que le métabolisme de la rétine, son apport sanguin et sa consommation de l'oxygène sont plus élevés dans le noir (Riva C.E. et al. 1983, Wang L. et al. 1996, Tam B.M. and Moritz O.L. 2007). Les stimuli physiologiques jouent supposément un rôle important dans le développement des différents systèmes nerveux (Arthur W. Spira, David Parkinson 1991). La privation de la rétine de son stimulus physiologique, la lumière, est un moyen valable de démontrer la validité de ce concept. D'autres études ont affirmé que les injections de dichlorure de paraquat dans la cavité vitréenne causent une sévère rétinopathie (Rétinopathie induite par paraquat: RIP). Cette rétinopathie est provoquée par les dérivés réactifs de l'oxygène (DRO) générés par le paraquat (Cingolani C. et al. 2006, Lu L. et al. 2006).

Le but de notre premier projet (''Dark rearing project'') était de déterminer si les conséquences nocives de l'hyperoxie postnatale chez les rats albinos SD pourraient être amoindries en élevant une portée de rats au noir. Nos résultats suggèrent qu'une augmentation du métabolisme de la rétine causée par la déprivation de lumière chez les ratons, pourrait protéger ou masquer certains effets néfastes de l'hyperoxie postnatale.

Le but de notre deuxième étude (''Paraquat project'') était d'examiner les possibles points de similitude entre RIP et d'autres modèles de rétinopathies oxydatives étudiés présentement par notre équipe, à savoir: Rétinopathie induite par l'oxygène (RIO) et Rétinopathie induite par la lumière (RIL). Nos résultats suggèrent que l'injection de dichlorure de paraquat dans la cavité vitréenne cause des changements sévères de la fonction de la rétine, tandis que sa structure semble intacte. La sévérité de ces changements dépend inversement de la maturité de la rétine au moment de l'injection.

Mots-clés : [Le stress oxydatif, la fonction et la structure de la rétine, l'électrophysiologie de la rétine].

Abstract

In previous studies it has been shown that retinal metabolism, blood flow and oxygen consumption are significantly higher during dark adaptation (Riva C.E. et al. 1983, Wang L. et al. 1996, Tam B.M. and Moritz O.L. 2007). Physiological stimuli are supposed to play an important role in development of different neural systems (Arthur W. Spira, David Parkinson 1991). One way to demonstrate the accuracy of this statement is depriving the retina of its physiological stimulus: light. It has also been shown that an intravitreal injection of paraquat dichloride causes a severe retinopathy (Paraquat-Induced Retinopathy: PIR) resulting from the reactive oxygen species (ROS) that it generates (Cingolani C. et al. 2006, Lu L. et al. 2006).

The purpose of our first project (''Dark rearing project'') was to determine whether the harmful effects of postnatal hyperoxia in albino SD rats could be decreased by dark rearing the rats. Our results would suggest that the increase in the retinal metabolic rate triggered by the dark-rearing period, would protect (or mask) some of the deleterious effects of postnatal hyperoxia.

The purpose of our second study (''Paraquat project'') was to examine how the PIR could be compared to the other models of oxidative

retinopathy currently studied by our team, namely: Oxygen-induced retinopathy (OIR) and Light-induced retinopathy (LIR). Our results suggest that an intravitreal injection of paraquat causes a severe functional but not structural retinopathy, the severity of which appears to be inversely related to the state of retinal maturation reached at time of injection.

Keywords: [Oxidative stress, retinal function and structure, retinal electrophysiology].

Table of content

LIST OF FIGURES

LIST OF TABLES

LIST OF ABBREVIATIONS

ABP: 2-amino-4-phosphonobutyric acid

AC: Amacrine cells

BB: Blue midget bipolar cells

BC: Bipolar cells

BRB: Blood-retina barrier

cGMP: Cyclic guanosine monophosphate

CNS: Central nervous system

DR: Dark reared

ERG: Electroretinogram

FMB: Flat midget bipolar cells

FRC: Free radical cascade

GABA: y-Aminobutyric acid

GC: Ganglion cells

HC: Horizontal cells

HSD: Honestly significant difference

IMB: Invaginating midget bipolar cells

INL: Inner nuclear layer

IPL: Inner plexiform layer

ipRGC: Intrinsically photosensitive ganglion cells

IS: Inner segment

KYN: Kynurenic acid

LGN: Lateral geniculate nucleus

LIR: Light-induced retinopathy

MC: Muller cells

MHC: Major histocompatibility complex

NADPH: Nicotiamide adnine dinucleotide phosphate

NC: Normal control

O_2: Oxygen

OIR: Oxygen-induced retinopathy

ONL: Outer nuclear layer

OPL: Outer plexiform layer

OPs: Oscillatory potentials

OS: Outer segment

P: Postnatal day

PBS: Phosphate-buffered saline

PDA: 2,3-piperidine-dicarboxylic acid

PIR: Paraquat-induced retinopathy

PL: Photoreceptor layer

ROP: Retinopathy of prematurity

ROS: Reactive oxygen spices

RPE: Retinal pigment epithelium

SD: Sprague-Dawley rats

Papa, j'aurais tellement aimé que

tu sois là...

Remerciements

Tout d'abord j'aimerais remercier l'Université de Montréal et tous les Professeurs que j'ai eu la chance de côtoyer tout au long de mes études à l'UdeM de m'avoir permis de poursuivre mon cursus académique et de m'intégrer si facilement au Québec.

Je remercie infiniment mon directeur de recherche Dr Sylvain Chemtob, qui a accepté de superviser mes études graduées. Je vous remercie Dr Chemtob, pour votre aide, vos précieux conseils et votre disponibilité.

J'aimerais également remercier mon codirecteur de recherche Dr Pierre Lachapelle qui m'a accepté au sein de son laboratoire et m'a fait découvrir l'électrophysiologie visuelle. Je te remercie Pierre pour ta patience, tes conseils et ton aide. Pour moi tu es plus qu'un professeur, je te considère comme un mentor et un ami. Durant les deux années que j'ai passées dans ton laboratoire, j'ai énormément appris non seulement sur l'électrophysiologie, mais aussi sur l'histoire et la culture québécoise, quelques recettes culinaires, mais c'est dommage que je n'ai pas eu le temps d'apprendre à skier!

Je remercie ma collègue de travail et amie Ania pour son aide précieuse. Tu as toujours été prête à m'assister même enrhumée, même samedi matin. Je remercie également Marie Lou, Wenwen, Julie, Allison et Hadi pour vos conseils. Merci à mes "roomies" préférés Malgosia, Mathieu et Simon.

Je ne remercierais jamais assez mes parents et ma sœur pour leur soutien et leur confiance; mon épouse Julie pour avoir toujours été à mes côtés durant les moments les plus difficiles, je te remercie d'avoir toujours cru en moi.

1 INTRODUCTION

According to the World Health Organisation's estimate, there are over 160 million people struggling from visual impairments, among them more then 30 millions are legally blind. The leading causes of visual loss and blindness are: cataracts, glaucoma, age-related macular degeneration (AMD), diabetic retinopathy, childhood blindness, trachoma, etc. The oxidative stress is thought to trigger numerous potentially blinding neurodegenerative diseases such as: the retinopathy of prematurity, age-related macular degeneration, glaucoma and diabetic retinopathy. The better understanding of the deleterious effects of the oxidative stress on the retinal function and structure is essential in order to develop efficient therapeutic avenues.

Therefore, the purpose of the present work was to study the functional and structural changes in different animal models of retinopathies induced by oxidative stress. In our first project, we studied the possible beneficial effect of dark rearing in the animals exposed to high levels of oxygen during their first two weeks of life. As for our second project, we studied the harmful effect of paraquat (N,N′-dimethyl-4,4-bipyridinium dichloride) injections on the retinal function and structure.

We hope that our work will arouse enough interest to trigger further studies regarding the involvement of oxidative stress in the development of retinopathies, in order to eventually initiate clinical trials and to discover effective cures.

1.1 **The retina**

The retina is a complex, layered tissue formed of five distinct types of neurons and one type of glial cell. In vertebrates, the retina is formed of three layers of neuronal cell bodies interconnected by two synaptic zones, the outer and the inner plexiform layers (Dowling, 1970).

In vertebrates, the retina is formed during the embryonic development from an outgrowth of the brain; consequently, it can be considered a part of the central nervous system (CNS). The retina is a unique part of the CNS that is accessible to non-invasive visualization (Kolb, 1994).

The first to describe and draw different cells and layers from vertebrate retina was the great Spanish anatomist, histologist and physiologist Santiago Ramon y Cajal. In the nineteenth century, he illustrated different vertebrate retinas using Golgi staining methods. Recent

progress in medical imagery, such as electron microscopy and microelectrode recording as well as evolution of pharmacology, have allowed better perception and comprehending of the retinal structure.

The visual processing in vertebrates undergoes two stages; the first one is the transduction of the image by the photoreceptors which generates a neural signal, the second is the transmission of this signal by the ganglion cells though their axons which form the optic nerve (Sernagor, 2005).

1.1.1 **Retinal cytoarchitecture**

The vertebrate retina is a complex photosensitive structure, about half a millimetre thick, coating the posterior surface of the eye (Kolb, 1994). The outer nuclear layer (ONL) is composed of photoreceptor (rods and cones) cell bodies, the inner nuclear layer (INL) includes cell bodies of the bipolar cells (BC), horizontal cells (HC) and amacrine cells (AC), and finally the ganglion cell layer contains ganglion cells (GC) and some "colonial" amacrine cells. These three neuronal layers are interconnected by two synaptic zones. The first is the outer plexiform layer (OPL), where the connection between rods and cones as well as vertically oriented bipolar cells and horizontally oriented horizontal cells occurs. The second synaptic layer is the inner plexiform layer (IPL) where the neuronal signal is

transmitted by bipolar cells to the retinal ganglion cells. Finally, ganglion cell axons forming the optic nerve relay the neuronal signal to the brain (Villegas, 1960).

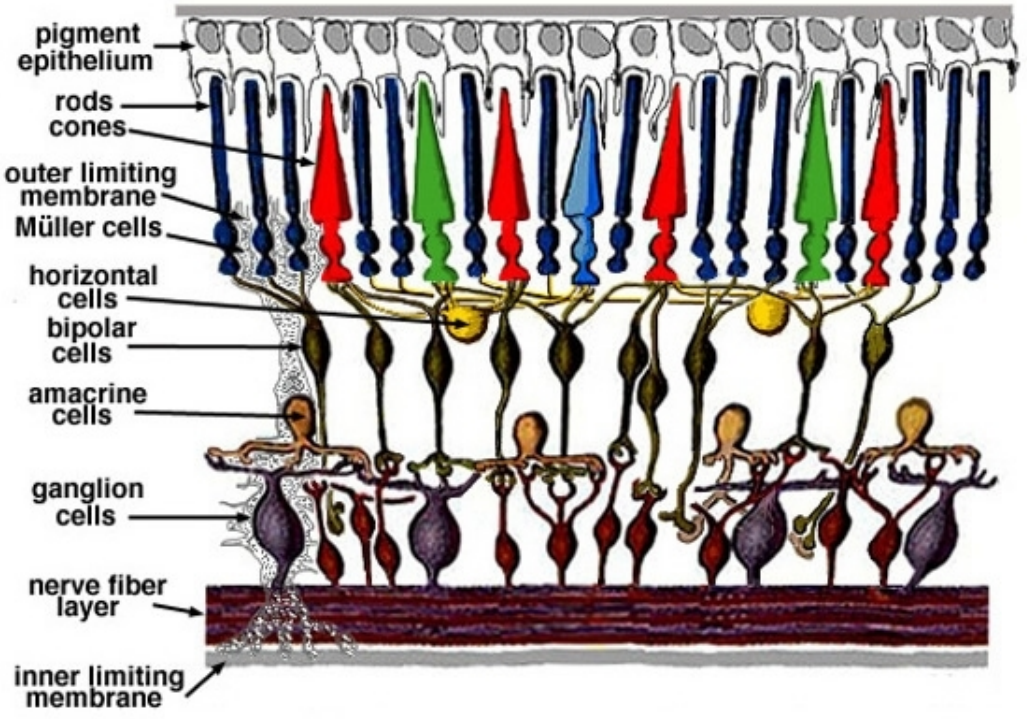

©http://webvision.med.utah.edu/sretina.html

Figure 1: Simplified schema of retinal structure

1.1.1.1 **Retinal pigment epithelium (RPE)**

The retinal pigment epithelium (RPE) contains a single layer of pigmented cells and is bordered at its apical surface by the photoreceptor outer segment and at its basal surface by the Buch's membrane. Due to its

particular location, the RPE is considered part of the blood-retina barrier (BRB) (Strauss, 2005).

The RPE plays numerous important roles in the homeostasis of the retina. The most important among countless functions of RPE are: light absorption and protection against oxidative stress; transport of nutrients; maintenance of normal visual cycle by reisomerization of all-trans-retinal into 11-cis-retinal and preservation of subretinal ion balance which is crucial for normal photoreceptor function. Also, being part of the BRB, the RPE plays an important role in the maintenance of the particular immune system of the eye by the secretion of immunosuppressive factors, as well as, the expression of major histocompatibility complex (MHC) molecules, adhesion molecules and cytokines. These various and essential functions demonstrate the major importance of RPE for the normal visual function (Simo, 2009).

1.1.1.2 **Photoreceptor layer (PL)**

The vertebrate retina contains two types of photoreceptors: approximately 150 million rods and 7 million cones. Three essential functional parts can be identified in both types of photoreceptors: 1) The outer segment (OS) where the phototransduction occurs is located at the distal part of the retina. The OS is formed by piles of membranes

containing the visual pigment; 2) The inner segment (IS) positioned at the proximal part of the retina contains photoreceptor cell bodies and nuclei as well as mitochondria and ribosomes. The IS is also known to supply the outer segment with energy rich phospholipids; 3) Photoreceptor synaptic terminals where neurotransmission takes place (Kandel, Schwartz, & Jessell, 2000).

As mentioned earlier, vertebrate photoreceptors contain a visual pigment which is formed of a protein called opsin and a vitamin A derived chromophore called retinal. The photoreceptor visual pigment plays an essential role in the visual cycle which can be summarized by several steps: 1) A light photon activates the photoisomerisation of 11-cis retinal into all-trans retinal; this process activates cGMP phosphodiesterase and triggers the reduction of cGMP concentration in the cytoplasm which causes the closure of cGMP-gated channels, and consequently hyperpolarizing the photoreceptor (Hargrave, McDowell, 1992; Kawamura, 1995).

Previous studies have shown that rods contain a visual pigment called rhodopsin which is sensitive to blue-green light; due to their high sensitivity, rods are responsible for night vision. The peak sensitivity of rods is about 500nm wavelength of light. On the other hand, cones contain a visual pigment called opsin and due to its different molecular structure,

cones are sensitive to long 564nm (red light), medium 533nm (green light) or short 437 nm (blue light) wavelengths of light. Furthermore, different types of cones will be designated as L, M and S-cones according to wavelength of light to which they are sensitive. Cones are known to be responsible for colour vision (Gouras, 1984; Dowling, 1987; Kolb 2003).

1.1.1.3 **Outer plexiform layer (OPL)**

Outer plexiform layer is the first synaptic zone located within the outer retina. The major part of the OPL is formed by the dendrites of the bipolar cells (Caceci 2001). OPL is a synaptic area where rod spherules and cone pedicles are interconnected with dendrites of vertically oriented bipolar cells and horizontally oriented horizontal cells (Mariani, 1981; Kolb, 1994).

1.1.1.4 **Inner nuclear layer (INL)**

Adjacent to the OPL is the inner nuclear layer which contains the nuclei of bipolar, horizontal, amacrine and Muller cells (Strettoi, Masland, 1995). Each of these cells will be described below.

1.1.1.5 **Horizontal cells (HC)**

In the mammalian retina, HC are laterally connected to the axon terminals of rods and cones as well as to the dendrites of bipolar cells. One of the most important functions of horizontal cells is to adjust vision under bright and under poor light conditions (Dacey, 1999; Razjouyan, 2009).

Previous studies have shown the existence of three morphologically different horizontal cells (HI, HII and HIII) in primates, but their exact function is still controversial.

For example, while Boycott and Wassle (1991) suggested that HI and HII cells are nonselectively connected to all types of cones, Anhelt and Kolb (2000) have shown that HI cells are mostly connected to L, M and only to a small amount of S-cones, and that HII cells are selectively linked to S-cones. According to Kolb (2003), HIII cells are morphologically similar to HI cells, but are connected only to L and M-cones. .

1.1.1.6 **Bipolar cells (BC)**

Bipolar cells are located in the INL and are responsible for transfer of visual signal from photoreceptors and horizontal cells to ganglion cells. BCs are connected through their dendrites to either cones or rods. More specifically in the mammalian retina, numerous studies have shown ten

types of cone-BC and only one type of rod-BC. Depending on how they respond to glutamate released by hyperpolarized photoreceptors, BC are divided into ON (depolarizing) or OFF (hyperpolarizing) BCs (Forrester, 2002).

In primates, two major types of bipolar cells are identified: diffuse bipolar cells and midget bipolar cells. While diffuse bipolar cells are known to be connected to several different cones, midget bipolar cells are synaptic to only one cone (Dacey, 1999).

Furthermore, midget BCs are subdivided into three different types: invaginating midget bipolar (IMB) cells, flat midget bipolar (FMB) cells and finally blue midget bipolar (BB) cells (Kolb, 1970; Forrester, 2002). The IMB cells are characterized by creating synaptic contact with every invagination on the cone pedicles, while the FMB cells create only a superficial bind with the cone pedicles. Finally BB cells were first identified and described by Kouyama and Marshak in 1992 and are distinguished by their selectivity to S-cones (Kolb, 1992).

1.1.1.7 **Amacrine cells (AC)**

Amacrine cells are large interneurons with a rich synaptic network, which are located in the inner part of the INL. About 40 different morphological types of amacrine cells have been described in the mammalian retina. Depending on the depth of their dendritic stratification in the IPL, AC are subdivided into diffuse or stratified amacrine cells. ACs can also be classified according to their neurotransmitters, such as GABA or glycine for example. ACs play an important role in motion detection and adjusting of visual image brightness (Kidd, 1962; Kolb, 1994; Forrester, 2002).

1.1.1.8 **Muller cells (MC)**

MC constitute the principle glial cells in the vertebrate retina, and they are the only cells that span the entire thickness of the retina, thus connecting the outer and the inner limiting membranes of the retina.

MC assure numerous crucial functions such as: to supply the retinal neurons with nutrients through glucose metabolism; to maintain the retinal ion and water homeostasis; to form the retinal-blood barrier; to eliminate neuronal waste products; to recycle neurotransmitters and finally to support the structural architecture of the retina (Bringmann et al., 2006).

1.1.1.9 **Inner plexiform layer (IPL)**

The IPL is a synaptic zone located between the INL and GCL. The IPL contains Muller cell fibres and numerous processes of bipolar, amacrine and ganglion cells.

The IPL is functionally divided into the distal sublamina where synaptic connections between OFF-bipolar cells and ganglion cells occur and the proximal sublamina where ON-bipolar cells synapse with ganglion cells dendrites (Pickard et al., 2009).

1.1.1.10 **Ganglion cells (GS)**

More then 20 different morphological types of GCs have been described in the primate retina. While the nuclei of GCs form the last nuclear layer of the retina, their axons constitute the optic nerve. The ganglion cells collect and transmit the visual information from the retina to the lateral geniculate nucleus (LGN) in the thalamus through the optic nerve. The GCs play an essential role in adjustment of contrast, colour vision, motion detection and three dimensional perception (Boycott, Wassle, 1974; Kolb, 1992; Pickard et al., 2009).

In the primate retina, numerous morphologically and physiologically distinct types of GC have been identified. The most studied among RGC are M and P types of ganglion cells, which respectively project to the magnocellular and parvocellular areas of the LGN.

P-ganglion cells, also known as midget ganglion cells, are medium-sized cells synaptic to amacrine and midget bipolar cells. They are responsible for colour vision and contrast adjustment. M-ganglion cells, also referred to as parasol ganglion cells, are bigger in size and have a larger synaptic network and are in charge of motion detection (Kaplan, Benardete, 2001).

According to recent studies, there is a third type of retinal ganglion cell that synthesizes the photopigment melanopsin and reacts to the light stimulus by depolarization. These types of ganglion cells are referred to as intrinsically photosensitive GC (ipRGC). It has been observed that ipRGCs create a strong synaptic contact with bipolar and amacrine cells (Pickard et al., 2009; Kolb, 2001).

1.1.2 **Light induced electrical events and retinal physiology**

1.1.2.1 **Phototransduction**

Phototransduction is a complex cascade of events through which a photon is converted into an electrical signal in photosensitive retinal cells such as rods, cones and ipRGCs.

In dark conditions, the photoreceptors are maintained in depolarized state while their membrane potential is approximately -40 mV. The depolarization of photoreceptors in darkness occurs through so called "dark current". Dark current consists of two major currents: the influx of Na^+ and Ca^{2+} through cGMP-gated channels situated in the OS membrane; and the efflux of K^+ through non-gated K^+-selective channels located in the IS. Interestingly, in dark conditions when the photoreceptor membrane is depolarized, the cytoplasmic concentration of cGMP is higher, which allows cGMP-gated channels to stay open and therefore to maintain the dark current (Purves et al., 2001).

It is well known that rods contain a photosensitive visual pigment called rhodopsin. Rhodopsin is formed of two components: a protein opsin and a light absorbing derivate of vitamin A: retinal. The retinal has several isomeric configurations, two of which play an essential role in the visual cycle.

After photon absorption, the 11-cis retinal is transformed into all-trans retinal, which causes conformational modification of the opsin into its

active form metarhodopsin II. Being extremely unstable, metarhodopsin II undergoes division into opsin and all-trans retinal. Further, opsin activates transducin, which is a regulatory protein, and causes the bind of alpha-subunit of transducin with GTP. The association of alpha-subunit with GTP triggers the activation of cGMP phosphodiesterase which results in the breaking down of cGMP to 5'-GMP. The decrease of cytoplasmic concentration of cGMP causes the closure of cGMP-gated channels. This cascade results in the hyperpolarization of the photoreceptor membrane which reaches a potential of -70 mV.

The end of the phototransduction cascade occurs when the rhodopsin is deactivated by the opsin kinase through the phosphorylation process. Next, the phosphorylated rhodopsin binds with a protein called arrestin which stops its interactions with the transducin. The transducin is then inactivated by the hydrolysis of GTP to GDP which activates the guanylate cyclase and restores cGMP concentration (Arshavsky, 2002).

1.1.2.2 **ON- and OFF-pathways**

It has been already mentioned that in dark conditions, retinal photoreceptors are depolarized and constantly release glutamate, and once exposed to the light, the photoreceptors become hyperpolarized and cease the glutamate secretion.

Bipolar cells which transfer the visual information from photoreceptors to ganglion cells are classified into two distinct groups, ON- and OFF-bipolar cells, depending on how they react to glutamate released by the photoreceptors. When hyperpolarized photoreceptors stop glutamate secretion, ON-bipolar cells depolarize through the metabotropic receptor; on the contrary, OFF-bipolar cells become hyperpolarized through ionotropic receptors. Furthermore, ON- and OFF-bipolar cells transmit the visual information to ON- and OFF-ganglion cells respectively, creating two distinctive circuits of cone pathways. It has been shown that cone pathways are responsible for contrast vision (Margolis et al., 2010; Liang, Freed, 2010).

While cones are synaptic to two types of bipolar cells (ON-BC and OFF-BC), rods make connections only with ON-bipolar cells. These rod bipolar cells do not contact any ganglion cell directly, instead, they create ribbon synapses with two types of amacrine cells: A II and A 17. A II amacrine cells transmit the visual signal from rod bipolar cells to OFF-center ganglion cells through the glutamatergic synapses. They also create a link between rod and cone pathways by sending rod-generated visual signal to the cone bipolar cells through gap junctions and thus to ON- and OFF-center ganglion cells. A 17 amacrine cells are thought to interconnect a large number of rod bipolar cells. This large synaptic network may play

an important role in amplifying visual signal under poor light conditions (Kolb, 2001).

1.2 **The electroretinogram (ERG)**

The ERG is a recording of mass electrical response produced by the retina to light stimulation. The first ERG was recorded in 1865 by Holmgren, who observed a change in the electrical potential of the frog eye in response to a light stimulus. Later, in 1880 he suggested that the retina was the origin of this phenomenon. In 1877, the first human ERG was recorded by Dewar. In 1903, Glotch was the first to describe the morphology of ERG and dissociate it into two consecutive deflections: negative and positive. Five years later, in 1908, Einthoven and Jolly separated ERG into three distinctive waves and named them a, b and c waves respectively. Later on, work by Granit (1933), Morton (1954) and Yonemura (1962) contributed to the better understanding of retinal electrophysiology (Rouck, 1991).

1.2.1 **Components of the ERG**

First attempts to describe and classify the different elements of the ERG were done more then one hundred years ago. A century later, our

understanding of electroretinogram was enriched by numerous studies, but still is not complete. Three major elements of flash ERG such as a-wave, b-wave and oscillatory potentials will be described in details below.

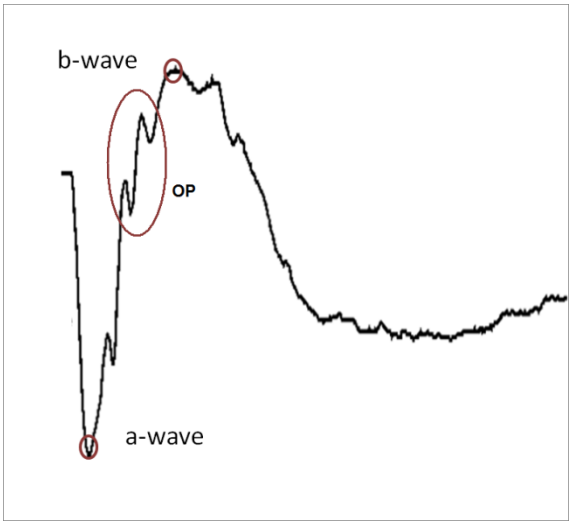

Figure 2: Typical scotopic mixed rod-cone flash ERG

1.2.1.1 **a-wave**

The a-wave is an initial, negative in polarity component of ERG which is triggered by hyperpolarisation of the photoreceptors in response to the light stimulus (Asi, Perlman, 1991). However, the role of photoreceptors as the unique generators of the ERG a-wave was questioned by numerous studies. For example, Bush and Sieving (1994) performed intravitreal injections of PDA (2,3-piperidine-dicarboxylic acid) in primates in order to obstruct the response of BC and HC to light stimulus.

They have shown that following PDA injections, a slight decrease of a-wave amplitude occurred, that would suggest that a-wave could have some postreceptoral origins. Similar results were obtained by injections of aspartate, a glutamate analog, which is known to nonselectively suppress all postsynaptic light-induced activity. The injection of cobalt, which blocks postsynaptic light evoked responses through Ca^{++} dependant synaptic vesicular release, also resulted in significant decrease of the a-wave. Later on, Jamison et al. (2001), also using inrtavitreous injections of PDA, were not able to exclude the possibility of postreceptoral contribution to a-wave. Paupoo et al. (2000), performing human ERG recordings, also concluded that some postreceptoral mechanisms may play a role in the a-wave structure.

1.2.1.2 **b-wave**

The b-wave is a positive in polarity component of the ERG. It is thought that the main generators of b-wave are Muller cells and bipolar cells, but this statement is still controversial.

The role of the Muller cells as direct generators of a b-wave have been proposed by numerous studies. The "Current source density" analysis performed by Faber in 1969 have shown that the generation of the b-wave is triggered by ionic fluxes across the MCs membranes. It was

proved, based on several studies, that MC membranes are selectively permeable to potassium (Newman, 1984; Newman, 1985). Further studies have suggested that the depolarization of the retinal neuronal cells increases the extracellular potassium concentration which produces currents alongside the Muller cells and thus generates the b-wave (Newman, Odette, 1984). Later on, this suggestion was confirmed by studies performed by Wen and Oakley (1990) on Bufo marinus isolated retinas. "Muller cell/Potassium current" hypothesis was also supported by intraretinal injections of potassium which resulted in potential changes of the Muller cell membrane related to the b-wave (Fujimoto, Tomita, 1981; Yanagida, Tomita, 1982). Also, the important role played by MCs in the generation of b-wave was suggested by the fact that DL-alpha amino adipate, which is a Muller cell toxin, causes a complete loss of the b-wave (Bonaventure et al., 1981).

Stockton and Slaughter (1989) have proven the participation of BCs in shaping of b-wave in amphibians. They observed the loss of b-wave caused by ABP application (2-amino-4-phosphonobutyric acid) which is known to selectively abolish the ON-bipolar cell function. On the contrary, PDA as well as KYN (kynurenic acid), which are known to block the light induced responses of the horizontal, OFF-bipolar and the third-order retinal neurons did not cause any changes to the b-wave amplitude.

1.2.1.3 **Oscillatory potentials (OPs)**

The OPs are light evoked high frequency and low amplitude waves located on the ascendant surface of the b-wave. Even though inner retina is thought to be the source of OPs, the exact mechanisms underlying the generation of OPs are still unclear (Genest, 1964).

Wachtmeister and Dowling (1978) have observed that short-latency OPs were generated in proximal and long-latency OPs in distal retina which would suggest that different oscillatory peaks may have different origins. Their studies in the mud puppy retina have revealed that oscillatory potentials were selectively suppressed by GABA, glycine and glutamate. Interestingly, acetylcholine nor carbacholine affected OPs. According to these results, they proposed that oscillatory potentials may represent retinal feedback oscillations. Later on, Guité and Lachapelle (1990) suggested that ON-bipolar cells may play an important role in shaping of the OPs. Using intravitreal injections of 2-amino-4-phosphonobutyric acid, they observed not only an expected decrease in b-wave amplitude, but also a rapid reduction of oscillatory potential amplitude. Later on, this tight connection between b-wave and OPs generators was confirmed by injecting a single dose of iodoacetic acid to adult New Zealand rabbits. Post injection ERG recordings revealed progressive loss of the b-wave and the long-latency OPs (Lachapelle et al., 1990).

While numerous studies confirm the existence of multiple origins of oscillatory potentials, Bui et al (2002) suggested that OPs were triggered by a single generator and that existence of multiple sources could be explained by contamination by the a-wave.

In 2004, Dong, Agey and Hare classified OPs recorded from Dutch-belted rabbits into three subgroups: early, intermediate and late OPs. Using intravitreal injection of diverse pharmacological substances in order to block different receptors and membrane channels, they attempted to determine the exact source of OPs. According to their results, oscillatory potentials are generated mostly by photoreceptors and by synaptic interactions between third order neurons. On the other hand, ON-BC and HC are thought to play a lesser role in OPs generation.

1.3 **Oxidative stress**

According to recent studies, oxidative stress is described as a misbalance between increased formation of pro-oxidant molecules and insufficient antioxidant defence mechanisms (Augustin et al., 2009). The retina is extremely vulnerable to oxidative stress due to its constant exposure to light as well as the high concentration of polyunsaturated fatty acids in its cell membranes. Overproduction of reactive oxygen species (ROS), caused by lipid peroxidation, triggers a free radical cascade (FRC).

The products generated by FRC are extremely harmful for the different components of retinal cells (Terrasa et al., 2009; Du, Gebicki, 2004). Oxidative damage is thought to be the cause of numerous retinal neurodegenerative diseases. In our laboratory, we mainly use two animal models of retinopathies induced by oxidative stress: light- and oxygen-induced retinopathies. Both of these models will be described below.

1.3.1 **Light-induced retinopathy (LIR)**

Light-induced retinopathy is caused by exposing the animals to bright light for different time periods. The severity of the impact of bright light exposure on retinal structure and function depends on the duration of exposure, the intensity of light and the age of exposed animals. The deleterious effect of bright light on the retina has been mostly described and documented with albino Sprague-Dawley (SD) rats.

In adult SD rats, even a short period (1 day) of exposure to bright (10000 lux.) light causes significant damage to the retinal structure such as a decrease of OS and IS as well as ONL and OPL thickness. The severity of structural damage is proportional to the exposure time. For example, after 6 days of exposure to bright light (10000 lux.), the complete degradation of OS, IS and OPL as well as further thinning of ONL was observed. Retinal functional damage triggered by bright light is always

accompanied by structural changes. A short period of exposure to bright light results in a significant reduction of all ERG components (mixed rod-cone a- and b-waves amplitudes, rod V_{max} and cone b-wave). An increase of the exposure time period causes complete loss of mixed rod-cone a-wave and a dramatic decrease of mixed rod-cone and photopic b-waves. In juvenile SD rats, the damage to retinal structure and function caused by exposure to bright light is less severe then in adults (Joly et al., 2006; Dorfman et al., 2009).

1.3.2 **Oxygen-induced retinopathy (OIR)**

Oxygen-induced retinopathy is a well studied animal model of retinopathy of prematurity (ROP), which is a potentially blinding disease. Prematurely born infants are usually exposed to high level of supplemental oxygen for medical reasons. Numerous studies have shown that postnatal hyperoxia triggers the obliteration of retinal blood vessels and the interruption of normal vascularisation in the peripheral retina. Further, in normoxia conditions, vessel-deprived peripheral retina undergoes an ischemic reaction which triggers abnormal neovascularisation (Barnet et al., 2009; Dembinska et al., 2000).

The hallmark of OIR is the alteration of retinal vasculature which consists in a decrease of vascular density in peripheral retina and an

increase of vascular tortuosity. Such changes can be easily observed using fundus photography or retinal flat mounts (Akula et al., 2008).

It has been reported that exposure to the high level of oxygen (80%) during the first two weeks of life causes severe damage to retinal structure, such as a decrease of the amount of HCs and a loss of OPL.

Functional impairment caused by postnatal hyperoxia consists of a reduction of ERG wave amplitudes. While the scotopic and photopic b-wave amplitudes are dramatically reduced, the a-wave is far less affected (Dembinska et al., 2000). It should be noted that the gravity of retinal functional and structural damages is strain-dependant and is more pronounced in pigmented Long-Evans (LE) rats then in albino SD animals (Dorfman et al., 2010).

2 PROJECTS

2.1 Materials and methods

2.1.1 Animals

Our projects were approved by the Montreal Children's Hospital Research Institute according to the directives of the Canadian Council on Animal Care and were performed in accordance with the ARVO Statement for the Use of Animals in Ophthalmic and Vision Research.

In the present studies, albino Sprague-Dawley rats were used. For the "Dark rearing study", dark reared albino SD pups (Charles River Laboratories, St. Constant, Quebec, Canada) were housed with their mothers in a hyperoxic (80% O_2) environment from postnatal day P0 to postnatal day P14 (DRO_2 group) (mixture of medical grade 100% oxygen and room air was measured with an oxygen meter ($MaxO_2$ Ceramatec, model OM25-ME; Medicana Inc., Montreal, Quebec, Canada)). Exposure to high levels of oxygen was maintained for 22,5 hours per day and was interrupted three times a day for 30 minute periods of normoxia (21% O_2). All manipulations, such as exposure interruptions, cage changes and oxygen tank changes, were performed under red light. Further, pups from

DRO_2 group (n=6) were compared to normal pups that were dark reared from postnatal day P0 to postnatal day P14 (DR14 group n=6) or from postnatal day P0-to postnatal day P28 (DR28 group n=8). At the end of the dark rearing period, all the animals were returned to a normal light environment (80 lux.). All groups were compared to age matched pups raised in normal light conditions (NC group n= 10).

For the "Paraquat project", the right eye of all Sprague-Dawley rats (n=12 per group) aged 7 (P7 group), 14 (P14 group) and 21 (P21 group) days old were injected with 1µl of 0.75mM of Paraquat dichloride (Sigma-Aldrich, St. Louis, MO) diluted in 0.1M PBS. The fellow (control) eyes were injected with the vehicle (PBS) only. The intravitreous injections were performed using a Hamilton microsyringe (Hamilton Company, Reno, NEV). The rats were anesthetised with an intramuscular injection of ketamine hydrochloride (85 mg/kg) and xylazine (5 mg/kg) and, using the dissecting microscope, the needle of the microsyringe was inserted into the vitreous cavity through the sclera just behind the limbus.

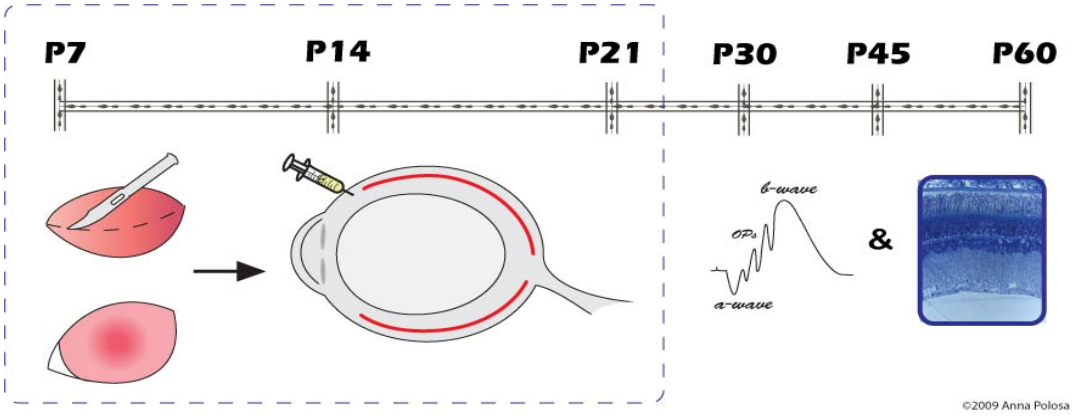

Figure 3: Time course of paraquat project

2.1.2 **Electroretinography**

In order to evaluate the effects of postnatal hyperoxia and the effects of dark rearing as well as the consequences of the paraquat injections on the retinal function, the ERGs were performed (AcqKnowledge Data Acquisition System, Biopac MP 100WS; Biopac Systems Inc., Goleta, CA) at postnatal days 30 and 60 for the "Dark rearing project" and at postnatal days 30, 45 and 60 for the "Paraquat project". Prior to the ERG recordings, the animals were dark adapted during a 12 hour period. Following the dark adaptation period, the rats were anesthetised under dim red light illumination with an intramuscular injection of ketamine hydrochloride (85 mg/kg) and xylazine (5 mg/kg). The cornea was anesthetised with two drops of 0.5% proparacaine hydrochloride solution (Alcaine; Alcon Laboratories Inc., Fort Worth, TX) and the pupils were dilated with two drops of 1% cyclopentolate hydrochloride solution (Mydriacyl; Alcon Laboratories Inc., Fort Worth, TX). The rats were then placed lying on their side in a Ganzfeld recording chamber which contained a photostimulator and a background light. The ERGs were recorded using three electrodes: a DTL fibre electrode (27/7 X-static silver-coated conductive nylon string; Sauquoit Industries, Scranton, PA) was placed on the cornea of each rat and served as an active electrode; a needle electrode (model E-2; Grass Instruments, Quincy, MA) was inserted into the animal's tail and served as a ground electrode; finally,

a disc electrode (model E6GH; Grass Instruments, Quincy, MA) was placed in the rat's mouth serving as a reference electrode. Hydroxymethylcellulose 2% (Gonioscopic solution; Alcon Laboratories) was applied on the cornea to prevent its desiccation and to immobilise the DTL.

First, scotopic luminance-responses were evoked to flashes of light stimuli spanning a 7.2 log-unit range (0.3 log-units increments; average, 3-5 flashes; interval between stimuli, 10.24 seconds; maximal intensity, 0.6 log cd.s/m^2). Then, photopic responses were recorded (flash intensity, 0.9 log cd.s/m^2; average, 20 flashes; interstimulus interval, 1 second; background light 30 cd/m^2) twenty minutes after adaptation to the background light.

2.1.3 **Retinal histology**

One day following the ERG recordings (at p30 and p60 for "Dark rearing project" and at p30, p45 and p60 for the "Paraquat project"), the rats were sacrificed by intraperitoneal injection of a lethal dose of anesthetic. Immediately following the sacrifice, the intracardiac perfusion of 3.5% glutaraldehyde in 0.067 M Sorensen Phosphate buffer was performed. The rat's eyes were then enucleated and kept in 3.5% glutaraldehyde for one hour. Under the dissecting microscope, the corneas

and lenses of each eye were removed and the remaining eye cups were fixed in 1% osmium tetroxide solution for four hours. Later, the eye cups were dehydrated in 50%, 70%, 90%, 95% and 100% ethanol baths and embedded in epoxy resin (Epon; Resolution Performance Products, Houston, TX). Histological sections 1µm thick were mounted on the glass slides and stained with 0.1% toluidine blue. The obtained images were studied and photographed using a Zeiss camera (Acti; Zeiss, Oberkochen, Germany) mounted on the microscope (Eclipse E-600; Nikon, Tokyo, Japan). For each animal, the thickness of each retinal layer was measured and analysed on six randomly chosen histological sections.

2.1.4 **Data analysis**

The amplitudes of all ERG components were analysed according to standard protocol. The amplitude of the a-wave was measured from the baseline to the most negative point while the amplitude of the b-wave was calculated from the most negative point of the a-wave to the most positive peak of the ERG. The photopic b-wave was measured from the baseline to the most positive point of the wave.

The b-wave amplitudes for each animal were then plotted against the corresponding flash intensities in order to create the scotopic luminance-response function curve. This luminance-response function

curve was then transformed into the sigmoidal regression curve (Prism IV. Windows addition; GraphPad Software, San Diego, CA) which was used to generate the rod V_{max} (maximum rod response without cone contamination). The mixed rode-cone response or the ERG response evoked by the highest flash intensity generated in scotopic conditions was also calculated. In order to compare the effects of postnatal hyperoxia or Paraquat injections on the retinal function and structure in different groups, the "one-way ANOVA" ($P<0.05$) and the "Tukey" (also known as "honestly significant difference" (HSD)) tests were used.

2.2 **Results**

2.2.1 **"Dark rearing project"**

2.2.1.1 **Effects of postnatal hyperoxia on the retinal function**

For the "Dark rearing project", dark reared albino Sprague-Dawley (SD) pups exposed to 80% oxygen from P0-P14 (DRO_2) were compared to normoxic (21% O_2) rat pups that were dark reared from P0-P14 (DR14) or P0-P28 (DR28) and to age matched pups raised in normal light conditions (NC). Figure 4 shows representative scotopic ERG waveforms obtained at

P30 from the different groups. In all studied groups, gradually increased stimulus flash intensity triggered a progressive augmentation of the a- and b-wave amplitudes. However, postnatal hyperoxia in the dark reared rats yield a significant decrease of the a- and b-wave amplitudes compared to the age matched animals, the whole independently from their rearing conditions. The amplitude attenuation of the scotopic ERG responses observed in the hyperoxic group is better illustrated in Figure 5-a (top) and 5-b (bottom) where the respective amplitudes of the a- and b-waves were fitted to sigmoidal dose-response curves. The same result is shown in Figure 6-a (top) and 6-b (bottom) where the mean values of the a- and b-wave amplitudes which were evoked by highest flash intensity (0.9 log cd.s/m^2) are compared in the different groups. These findings are also supported by the group data which shows a significant decrease of the a-wave (NC: 474.22 ± 81.35 µV; DR14: 415.04 ± 33.34 µV; DR28: 691.26 ± 82.91 µV; DRO_2: 310.81 ± 24.24 µV; $P < 0.05$) as well as the b-wave (NC: 1104.12 ± 134.11 µV; DR14: 1118.66 ± 46.41 µV; DR28: 1491.08 ± 39.62 µV; DRO_2: 616.15 ± 125.43 µV; $P < 0.05$) in oxygen-exposed rats compared to the dark reared control groups or the NC group. Similarly, the amplitude of the rod V_{max} calculated at P30 showed a significant decrease in the DRO_2 group (NC: 531.76 ± 77.2 µV; DR14: 536.90 ± 92.69 µV; DR28: 764.86 ± 112.02 µV; DRO_2: 306.93 ± 93.26 µV; $P < 0.05$). A comparison between mean values of the rod V_{max} of hiperoxic and control groups obtained at postnatal day 30 is graphically represented in Figure 7.

Similarly, the photopic b-wave of SD rats exposed to high levels of oxygen for the first two weeks of life was also significantly affected. Compared to the normoxic rats raised in normal light conditions (NC) and the dark reared control rats (DR28 and DR14), an important decline of the photopic b-wave amplitude occurred in dark reared oxygen-exposed rats (DRO_2) at postnatal day P30 (Figure 8). These results were once again confirmed by the group data (NC: 211.25 ± 36.41 μV; DR14: 238.80 ± 38.94 μV; DR28: 246.01 ± 16.03 μV; DRO_2: 109.82 ± 25.14 μV; $P < 0.05$).

As illustrated in Figures 9, 10a (top) and 11a (top), the scotopic ERGs recorded from the same animal groups at postnatal day P60, failed to reveal any significant changes of the a-wave amplitude in the DRO_2 group compared to the dark reared control groups (DR14: 346.45 ± 18.83 μV; DR28: 315.66 ± 28.03 μV; DRO_2: 345.20 ± 17.46 μV). Interestingly, the a-wave amplitude of NC rats was significantly decreased compared to dark reared oxygen exposed animals (NC: 235.31 ± 35.95 μV; DRO_2: 345.20 ± 17.46 μV; $P < 0.05$). The ERGs recorded at P60 have shown that postnatal hiperoxia caused an important decrease of the b-wave amplitudes in the DRO_2 compared to the control groups (Figure 9, 10b and 11b). These results were confirmed by the group data analysis (NC: 626.64 ± 69.56 μV; DR14: 816.53 ± 13.06 μV; DR28: 889.57 ± 23.13 μV; DRO_2: 504.87 ± 5.36 μV; $P < 0.05$). A similar tendency was observed for the rod V_{max} of the DRO_2 group, where a significant decrease of the amplitudes was noted

compared to the other groups. These results are illustrated in Figure 12 where the mean values of the rod V_{max} amplitudes of the different groups are graphically represented. The rod V_{max} amplitude attenuation in oxygen exposed SD rats was further confirmed by the group data analysis (NC: 471.63 ± 87.01 µV; DR14: 297.06 ± 18.23 µV; DR28: 536.63 ± 9.70 µV; DRO_2: 280.43 ± 102.25 µV).

Similarly, the photopic b-wave of the dark reared SD rats exposed to postnatal hyperoxia (DRO_2 group) was also significantly decreased at P60 (NC: 222.58 ± 41.27 µV; DR14: 220.57 ± 16.64 µV; DR28: 212.19 ± 18.29 µV; DRO_2: 108.79 ± 37.99 µV; $P < 0.05$). This data is graphically reported in Figure 13.

2.2.1.2 **Effects of dark rearing on the retinal function**

Table 1 shows the amplitude measurements of all ERG parameters (scotopic a- and b-wave, rod V_{max} and photopic b-wave) obtained from two out of four experimental groups at postnatal days P30 and P60. The first group shown in Table 1 represents the SD albino rats raised in room air (21% O_2) under normal light conditions (NC group). It is compared with dark reared (28 days) animals raised in normoxic environment (DR28 group). At postnatal day P30, our data shows a significant ($P < 0.05$)

augmentation of the scotopic and photopic b-waves, scotopic a-wave, and rod V_{max} in the DR28 group compared to the NC group.

The comparison of the ERG parameters obtained from the same groups at P60 shows similar significant ($P < 0.05$) increase of the a- and b-wave amplitudes in the DR28 group. There was also an insignificant ($P > 0.05$) rise of the rod V_{max}, however the amplitudes of the photopic b-wave failed to show any significant differences between those two groups (Table 1).

2.2.1.3 **Retinal cytoarchitecture**

Previous studies (Dorfman et al., 2006; Dembinska et al., 2002; Dembinska et al., 2000) have shown that the most important structural changes caused by postnatal hyperoxia in albino SD rats consist in almost complete disappearance of the OPL and a slight disorganisation of the ONL.

As shown in Figure 14, postnatal exposure to hyperoxia resulted in a significant ($P < 0.05$) thinning of the photoreceptor outer segment (OS) in the DRO_2 group compared to the NC rats. Interestingly, there were no significant changes in the ONL and the OPL between those same groups.

The representative retinal cross-sections obtained at P30 confirm these findings (Figure 15).

At P60, oxygen treated SD rats showed a significant ($P < 0.05$) thinning of the ONL, OPL and IPL compared to the NC animals. In contrast, the OS was better preserved in the oxygen-exposed rats (Figure 16 and 17).

In order to understand the impact of dark rearing on retinal cytoarchitecture, we compared the NC group to the DR28 group. As shown in Figures 14 and 15, the OPL as well as the IPL thickness are significantly increased in the dark reared control rats at postnatal day P30. However, the NC rats showed better preserved OS and ONL compared to the DR28 rats.

The same measurements done at P60 have shown that dark rearing of the normoxic rat pups from P0 to P28 resulted in significantly better preservation of the OS, OPL, INL and IPL. In contrast, no significant difference was observed in the ONL thickness of the NC group compared to the DR28 groups (Figure 16 and 17).

2.2.2 **"Paraquat project"**

2.2.2.1 **Effects of paraquat injections on the retinal function**

For the "Paraquat project", SD albino rats were intravitreously injected either with paraquat (right eye) or with PBS (left, control eye) at postnatal day P7, P14 and P21. ERGs were recorded from both eyes at P30, P45 and P60. The representative scotopic ERG waveforms recorded at P30 have shown that paraquat injections significantly hampered the normal development of the scotopic ERG waves in all the experimental groups. At each time point, the ERGs recorded from the paraquat injected eyes were of low voltage compared to the control eyes. However, the most remarkable outcome of the paraquat injection was reported in the P7 cohort where a total absence of any recordable scotopic response was observed at P30. Even amplification (10x) of the obtained waveforms failed to illustrate any retinal activity in this group (Figure 18). A significant ($P < 0.05$) amplitude attenuation of the scotopic a- and b-waves was also observed in the P14 and P21 groups compared with the control cohort. At postnatal day P30, the amplitude of the a- and b-waves of the P14 group was decreased by 23% and 41% respectively. On the other hand, in the P21 rats, this reduction was about 24% for the a-wave and 28% for the b-wave (Figures 19 and 20). A similar tendency was obtained for the rod V_{max} (Figure 21), where a significant attenuation in amplitude was observed in

the P14 (43%) and the P21 (27%) groups, while the rod V_{max} of the P7 rats remained unrecordable. Scotopic ERG waveforms obtained at P45 show a sudden apparition of ERG signal in the P7 group (Figure 22). At P45, a comparison between the scotopic parameters such as a-wave, rod V_{max} and rod-con b-wave of the paraquat treated and the control cohorts demonstrates a significant amplitude attenuation in the paraquat treated animals. The deleterious effect of the paraquat on the retinal function was further confirmed by the group data analysis (Table 3). The amplitude decrease of the a-wave for the P7, P14 and P21 groups was respectively 52%, 15% and 28%; the b-wave amplitude reduction was respectively 48%, 24%, 27%; the rod V_{max} attenuation was respectively 32%, 9% and 9%. A comparable trend was observed later on at postnatal day P60 Figure 23). All three paraquat injected cohorts showed a significant decline in the amplitude of the scotopic ERG parameters at P60 (Figures 19, 20 and 21). Following the paraquat injections at postnatal day P7, the amplitude reduction of the a-wave, b-wave and rod V_{max} was about 21%, 32% and 7% respectively. A more pronounced attenuation of the scotopic ERG parameters was observed in the P14 (13%, 41%, 11%) and P21 groups (52%, 62%, 53%) (Table 3). Interestingly, while comparing scotopic a- and b-wave amplitudes of all the experimental groups at different time points, we observed not only a gradual amplitude augmentation of all the scotopic ERG parameters of the P7 rats, but also a significant decrease of these parameters in the P21 group. On the other hand, at all instances, the

P14 group was less significantly affected compared to the P21 group (Figure 24).

The photopic b-wave of the paraquat treated rats was also strongly affected. There was no recordable photopic b-wave in the P7 group. Meanwhile, a significant decline of the photopic b-wave was observed in the regiments treated with paraquat at P14 and P21. Figures 25, 26 and 27 show a gradual increase in the amplitude of the photopic b-wave in the P7 group, which reaches its culminating point at P60. While the P14 group, once again, appears less affected, the P21 group underwent a striking decrease of its photopic b-wave amplitude. Figures 24 and 28 emphasises the amplitude changes of the all ERG parameters observed at different time points in the paraquat treated groups compared to the control group. These results also suggest that young animals (P7) injected with paraquat might have better recovery of their retinal function, while paraquat injection at a later stage (P21) results in progressive attenuation of the retinal function.

2.2.2.2 **Effects of paraquat injections on the retinal cytoarchitecture**

The representative retinal histologic sections obtained from the P7, P14 and P21 groups at postnatal days P30, P45 and P60 are shown in

Figure 29a-(left) and b-(right). Despite dramatic changes in the retinal function after the paraquat injections (especially in P7 group), retinal histology fails to reveal evidence of structural anomalies that could explain the functional impairment reported above. At all time points, the paraquat injected retinas appeared normal. The only morphologic irregularity, such as ONL invagination, was observed at postnatal day P30 in the P21 cohort (Figure 29). These infoldments were found in the central retina of two out of four rats 9 days following the paraquat injections. Previous studies (Cingolani C. et al. 2005) have shown that intravitreal injection of paraquat causes an important thinning of the ONL, especially in the central (posterior) retina. In order to determine whether this statement is accurate in our study, we performed quantitative measurements of the ONL thickness (Table 4). Compared to the control group, there was no significant changes of the ONL thickness in the paraquat treated cohorts.

3 DISCUSSION

Previous studies have shown that oxidative stress plays a very important role in the initiation of numerous neurodegenerative diseases. The retina is highly susceptible to oxidative stress because of its permanent exposure to light and also of the abundance of polyunsaturated fatty acids in its structure. The retinopathy of prematurity, age-related macular degeneration, glaucoma and diabetic retinopathy are believed to

be related or even triggered by oxidative stress (Drel, Sibrina, 2010; Pazdro, Burgess, 2010; Salminen et al., 2010; Augustin et al., 2009).

The retinopathy of prematurity (ROP) is a major cause of visual loss in infants, potentially leading to blindness. There is an inverse correlation between the gestation term, the infant's weight at birth and the risk of ROP. Premature infants born before 31 weeks of gestation and weighting 1250 grams or less are more susceptible to develop a ROP (Braverman, Enzenauer, 2010; Hellman, 1950). This was first described in the mid 1950s in the USA but it was only in the 1970's that the link between unmonitored oxygen administration to premature babies and development of ROP was discovered. From there on, in order to better understand the exact mechanisms underlying the development of ROP, several experimental animal models were studied (Gilbert et al., 1994). One of the best and most widely used animal model of ROP is oxygen induced retinopathy (OIR) in SD rat pups. As all altricial animals, rat pups are born with immature retina and their exposure at birth to high levels of oxygen perfectly mimics the deleterious effect of oxygen on premature babies. The hallmark of the OIR is an abnormal proliferation and tortuosity of the retinal vasculature accompanied by functional (dramatically attenuated scotopic and photopic b-waves) and structural (loss of OPL and decreased number of HCs) impairments (Akula et al., 2008; Penn et al., 1988; Dembinska et al., 2002).

In the dark, photoreceptor depolarization triggers inward Na^+ and Ca^{2+} current called "dark current". Dark current allows photoreceptors to constantly release neurotransmitter glutamate and thus to hyperpolarize rod BCs and on-cone BCs. Consequently, in the dark, retinal metabolism and oxygen consumption are strongly augmented (Saszik, Bilotta, 2001; Giovannelli et al., 2008). Even though previous studies relating to the impact of dark rearing on the retinal function and structure have had controversial results, we can presume that dark rearing could have a beneficial effect during the OIR. Our results have demonstrated that following the postnatal dark rearing period in normoxic rats, the amplitudes of all the ERG parameters were higher compared to the normoxic animals raised in normal light conditions. Our results show a pronounced increase of a- and b-wave amplitudes (45% and 35% respectively) in dark reared control animals compare to the NC rats at postnatal day P30. The amplitudes of the photopic b-wave as well as rod V_{max} recorded at the same period were also augmented (16% and 43% respectively) compared to the NC cohort. A similar tendency was observed at P60. In fact, the function of the scotopic a- and b-wave, photopic b-wave and rod V_{max} seemed to benefit from the postnatal dark rearing period. Our results presented in Table 1 show the amplitude augmentation of the scotopic a-wave (34%), scotopic b-wave (42%) and rod V_{max} (13%) of the DR28 group compared to the NC regiment, although the photopic b-wave was slightly higher in the NC animals. The retinal cytoarchitecture in the dark reared cohorts at P60 was also better preserved then in the NC group, which can

be confirmed by greater thickness of different retinal layer (Figure 16 and 17).

Interestingly, our results compared to those obtained by Dorfman et al. in 2009 show that postnatal hyperoxia induced in dark reared Sprague-Dawley rats has a less dramatic impact on the retinal function and structure then in those reared in normal light conditions. According to our results, postnatal hyperoxia significantly decreases all scotopic and photopic parameters of the dark reared SD rats, but they still seem to be better preserved compared to rats exposed to high levels of oxygen in normal light conditions. The comparison between all the ERG parameters obtained at postnatal day 30 and 60 from the SD rats exposed to hyperoxia (P0-P14) in the dark (DRO_2) and normal light conditions (O_2), is summarized in Table 2. By studying the retinal structure, our results show a significantly diminished (but still present) outer plexiform layer in the DRO_2 group, while Dorfman et al. (2009) reported a complete absence of the OPL in rats exposed to oxygen (80%) in normal light conditions.

Taken together, our results would suggest that the increase in the retinal metabolic rate triggered by the dark-rearing period, would protect (or mask) some of the deleterious effects of postnatal hyperoxia.

Paraquat, also known as paraquat dichloride, is a non-selective herbicide widely used in agriculture. First synthesized in 1882, paraquat was actively promoted by the US government in the mid 1960s to eradicate marijuana plantations in South America. Over ten years later, it was found that paraquat can be highly toxic for animals and human beings. It should be noted that paraquat toxicity is dose dependant and there are several routs of exposure such as inhalation, bare skin, eyes and ingestion. The capability of paraquat to catalyze the formation of reactive oxygen species (ROS) through NADPH dependant redox cycling mechanism is often used in medical research. Previous *in vivo* (four to six weeks old mice) studies have shown that intravitreous injections of paraquat results in severe retinopathy (Dong et al., 2006; Cingolani et al., 2006). According to the results obtained by Cingolani et al. (2006), the severity of paraquat induced retinopathy is dose and time dependant. The same study has reported markedly attenuated ERG waveforms in all experimental cohorts (0.5, 0.75 and 1 mM of injected paraquat) after 3, 7 and 14 days following the injections. However, the most dramatic functional (decrease of all ERG parameters) and structural (thinning of ONL, vacuolisation and folding of ONL) changes were observed 7 days after intravitreal injection of 0.75 mM of paraquat. They did not report any significant difference between animals injected with 0.75 mM and 1 mM of paraquat, 7 or 14 days following the injections.

To our knowledge, we were the first ones to intravitreously inject albino SD rats at one, two and four weeks of age with 0.75 mM of paraquat in order to perform ERG recordings and histological analysis at P30, P45 and P60. Paraquat injections have caused a significant attenuation of the retinal function at each time point. However, our results have shown that P7 cohort had a complete absence of any recordable ERG parameter at P30 (23 days after the injection). Interestingly, at P45 (38 days after the paraquat injection) an unexpected apparition of ERG waveforms were documented. The gradual rise of the scotopic a-and b-waves, photopic b-wave and rod V_{max} amplitudes in the P7 group continued at P60 (53 days post injection). In the P14 group, an expected decline of all the scotopic and photopic parameters at P30 (16 days after the paraquat injection) was followed by a slight augmentation of all amplitudes at P45 (31 days post injection). However at P60 (46 days after paraquat injection), a new attenuation of retinal function was observed. Unlike the P7 and the P14 groups, the rats injected with paraquat at postnatal day P21 were characterized by a gradual and irreversible decline of their retinal function (Figures 23, 25; Table 4). Surprisingly, the dramatic alterations of the retinal function caused by the paraquat toxicity were not followed by any significant modification of the retinal structure. The only structural abnormality, such as sporadic ONL folding in the central retina, was observed in the P21 group 9 days (P30) following the paraquat treatment. Our results suggest that an intravitreal injection of paraquat causes a severe functional but not structural retinopathy, the severity of which

appears to be inversely related to the state of retinal maturation reached at time of injection. These results differ from our OIR and LIR models where functional deficits are always accompanied with important structural impairments. The fact that there is no significant changes in the retinal structure but major changes in retinal function could suggest that, although the initial impact is at the receptor level, there might also be a second site of oxydative damage in the inner retina.

4 CONCLUSION

Despite the controversial results obtained by previous studies relating to the impact of dark rearing on the retina, our study has shown that a short period of postnatal dark rearing in albino SD pups may have a positive effect on the retinal function and structure. Also, according to our results, retinal damage caused by postnatal hyperoxia is less dramatic in dark reared animals compared to regiments exposed to hyperoxia in normal light conditions.

The results of our second project suggest that the retinopathy induced by intravitreous injections of paraquat dichloride is age related. The deleterious effect of paraquat on the retinal function is particularly severe in young animals with a less mature retina at the time of the injections. However, young rats have better chances of recovery, while

attenuation of retinal function caused by paraquat injections in older animals is gradual and irreversible. Unfortunately, we don't have any evidence if apoptosis plays any significant role in PIR. However, the preservation of retinal structure following the intravitreous injections of paraquat allows us to speculate that there might be a second site of action. Further studies are crucial for the further development and understanding of this model of retinopathy.

In summary, oxidative stress is a pathological state, in which the anti-oxidative mechanisms of the organism are insufficient to provide an adequate defence against an increased rate of reactive oxygen species (ROS). This condition triggers a free radical cascade, the products of which cause the caspase-dependent and caspase-independent mitochondrial apoptosis. Independently of its source, oxidative stress plays a very important role in the pathogenesis of numerous ocular diseases. Consequently, the further study of different types of oxidative stress and their impact on the retinal function and structure will allow us to develop new therapeutic avenues. To conclude, it would be interesting to use the results of the present study to examine the neuroprotective effects of different antioxidant treatments.

5 REFERENCES

Articles

1. Abrahan, C.E., Insua, M.F., Politi, L.E., German, O.L., Rotstein, N.P. (2009). Oxidative stress promotes proliferation and dedifferentiation of retina glial cells in vitro. *Journal of Neuroscience Research,* 87(4):964-77.

2. Akula, J.D., Mocko, J.A., Benador, I.Y., Hansen, R.M., Favazza, T.L., Vyhovsky, T.C., Fulton, A.B. (2008). The neurovascular relation in oxygen-induced retinopathy. *Molecular Vision,* 14:2499-508.

3. Akula, J.D., Mocko, J.A., Benador, I.Y., Hansen, R.M., Favazza, T.L., Vyhovsky, T.C., Fulton, A.B. (2008). The neurovascular relation in oxygen-induced retinopathy. *Molecular Vision,* 14:2499-508.

4. Asi, H., Perlman, I. (1992). Relationships between the electroretinogram a-wave, b-wave and oscillatory potentials and their application to clinical diagnosis. *Documenta Ophthalmologica,* 79(2):125-39.

5. Barnett, J.M., Yanni, S.E., Penn, J.S. (2010). The development of the rat model of retinopathy of prematurity. *Documenta Ophthalmologica, 120(1):3-12.*

6. Bonaventure, N., Roussel, G., Wioland, N. (1981). Effects of DL-alpha-amino adipic acid on Mfiller cells in frog and chicken retinae in vivo: relation to ERG b-wave, ganglion cell discharge, and tectal evoked potentials. *Neuroscience Letters,* 27(1):81-7.

7. Boycott, B.B., Wassle, H. (1974). The Morphological Types Of Ganglion Cells Of The Domestic Cat's Retina. *The Journal of Physiology*, 240(2):397-419.

8. Braverman, R.S., Enzenauer, R.W. (2010). Socioeconomics of retinopathy of prematurity in-hospital care. *Archives of Ophthalmology,* 128(8):1055-8.

9. Bringmann, A., Pannicke, T., Grosche, J., Franckem M., Wiedemann, P., Skatchkov, S.N., Osborne, N.N., Reichenbach, A. (2006). Müller cells in the healthy and diseased retina. *Progress in Retinal and Eye Research*, 25(4):397-424.

10. Bush, R.A., Sieving, P.A. (1994). A proximal retinal component in the primate photopic ERG a-wave. *Investigative Ophthalmology and Visual Science,* 35(2):635-45.

11. Cingolani, C., Rogers, B., Lu, L., Kachi, S., Shen, J., Campochiaro, P.A. (2006). Retinal degeneration from oxidative damage. *Free Radical Biology & Medicine,* 40(4):660-9.

12. Dacey, D.M. (1999). Primate retina: cell types, circuits and color opponency. *Progress in Retinal and Eye Research,* 18(6):737-63.

13. Dembinska, O., Rojas, L.M., Chemtob, S., Lachapelle, P. (2002). Evidence for Brief Period of Enhanced Oxygen Susceptibility in the Rat Model of Oxygen-Induced Retinopathy. *Investigative Ophthalmology & Visual Science,* 43(7):2481-90.

14. Dembinska, O., Rojas, L.M., Varma, D.R., Chemtob, S., Lachapelled P. (2001). Graded Contribution of Retinal Maturation to the Development of Oxygen-Induced Retinopathy in Rats. *Investigative Ophthalmology & Visual Science*, 42(5):1111-8.

15. Dong, A., Shen, J., Krause, M., Akiyama, H., Hackett, S.F., Lai, H., Campochiaro, P.A. (2006). Superoxide dismutase 1 protects retinal

cells from oxidative damage. *Journal of Cellular Physiology,* 208(3):516-26.

16. Dong, CJ., Agey, P., Hare, WA. (2004). Origins of the electroretinogram oscillatory potentials in the rabbit retina. *Visual Neuroscience,* 21(4):533-43.

17. Dorfman, A., Chemtob, S., Lachapelle, P. (2010). Postnatal hyperoxia and the developing rat retina: beyond the obvious vasculopathy. *Documenta Ophthalmologica*, 120:61–66.

18. Dorfman, A., Polosa, A., Joly, S., Chemtob, S., Lachapelle, P. (2009). Functional and structural changes resulting from strain differences in the rat model of oxygen-induced retinopathy. *Investigative Ophthalmology & Visual Science,* 50(5):2436-50.

19. Dorfman, A., Dembinska, O., Chemtob, S., Lachapelle, P. (2008). Early Manifestation of Postnatal Hyperoxia on the Retinal Structure and Function of the Neonatal Rat. *Investigative Ophthalmology & Visual Science,* 49(1):458-66.

20. Dorfman, A., Dembinska, O., Chemtob, S., Lachapelle, P. (2006). Structural and functional consequences of trolox C treatment in the rat model of postnatal hyperoxia. *Investigative Ophthalmology & Visual Science, 47(3):1101-8.*

21. Dowling, J.E. (1970). Organization of vertebrate retinas. The Jonas M. Friedenwald Memorial Lecture. *Investigative Ophthalmology and Visual Science,* 9: 655-680.

22. Drel, V.R., Sybirna, N. (July 2010). Protective effects of red wine on diabetes associated oxidative/nitrative stress in streptozotocin-diabetic rats. *Cell Biology International.* Repéré à: http://www.cellbiolint.org/

23. Du, J., Gebicki, J.M. (2004). Proteins are major initial cell targets of hydroxyl free radicals. The *International Journal of Biochemistry & Cell Biology*, 36(11):2334-43.

24. Fujimoto, M., Tomita, T. (1981). Field potentials induced by injection of potassium ion into the frog retina: a test of the current interpretations of the electroretinographic (ERG) b-wave. *Brain Research,* 204(1):51-64.

25. Genest, AA. (1964). Oscillatory potentials in the electroretinogram of the normal human eye. *Vision Research,* 4(11):595-604.

26. Gilbert, C.E., Canovas, R., Kocksch, R., Foster, A. (1994). Causes of blindness and severe visual impairment in children in Chile. *Developmental Medicine & Child Neurology,* 36: 334-43.

27. Giovannelli, A., Di Marco, S., Maccarone, R., Bisti, S. (2008). Long-term dark rearing induces permanent reorganization in retinal circuitry. *Biochemical and Biophysical Research Communications,* 365(2):349-54.

28. Gollisch T, Meister M. (2010). Eye Smarter than Scientists Believed: Neural Computations in Circuits of the Retina. *Neuron,* 65(2):150-64.

29. Guité, P., Lachapelle, P. (1990). The effect of 2-amino-4-phosphonobutyric acid on the oscillatory potentials of the electroretinogram. *Documenta Ophthalmologica,* 75(2):125-33.

30. Hartnett, M.E. (2010). The effects of oxygen stresses on the development of features of severe retinopathy of prematurity: knowledge from the 50/10 OIR model. *Documenta Ophthalmologica*, 120(1):25-39.

31. Hellman, L.M. (1950). Obstetrics. *Annual Review of Medicine,* 1: 219-230.

32. Jamison, J.A., Bush, R.A., Lei, B., Sieving, P.A. (2001). Characterization of the rod photoresponse isolated from the dark-adapted primate ERG. *Visual Neuroscience,* 18(3):445-55.

33. Kaneko, A. (1979). Physiology Of The Retina. *Annual Review of Neuroscience, 2: 169-91.*

34. Kidd, M. (1962). Electron Microscopy Of The Inner Plexiform Layer Of The Retina In The Cat And The Pigeon. *Journal of Anatomy*, 96:179-87.

35. Kolb H. (1994). The architecture of functional neural circuits in the vertebrate retina. The Proctor Lecture. *Investigative Ophthalmology and Vision Science,* 35(5): 2385-404.

36. Lachapelle, P., Benoit, J., Guité, P., Tran, C.N., Molotchnikoff, S. (1990). The effect of iodoacetic acid on the electroretinogram and oscillatory potentials in rabbits. *Documenta Ophthalmologica,* 75(1):7-14.

37. Liutkeviciene, R., Lesauskaite, V., Asmoniene, V., Zaliūniene, D., Jasinskas, V. (2010). Factors determining age-related macular degeneration: a current view. *Medicina (Kaunas)*, 46(2):89-94.

38. Lu, L., Hackett, S.F., Mincey, A., Lai, H., Campochiaro, P.A. (2006). Effects of different types of oxidative stress in RPE cells. *Journal of Cell Physiology,* 206(1):119-25.

39. Margolis, D.J., Gartland, A.J., Euler, T., Detwiler, P.B. (2010). Dendritic Calcium Signaling in ON and OFF Mouse Retinal Ganglion Cells. *The Journal of Neuroscience,* 30(21):7127-38.

40. Miyake, Y., Shiroyama, N., Ota, I., Horiguchi, M. (1988). Oscillatory potentials in electroretinograms of the human macular region. *Investigative Ophthalmology and Visual Science,* 29(11):1631-5.

41. Newman, E.A., Odette, L.L. (1984). Model of electroretinogram b-wave generation: a test of the K+ hypothesis. *The Journal of Neurophysiology,* 51(1):164–182.

42. Paupoo, A.A., Mahroo, O.A., Friedburg, C., Lamb, T.D. (2000). Human cone photoreceptor responses measured by the electroretinogram a-wave during and after exposure to intense illumination. *The Journal of Physiology,* 529 Pt 2:469-82.

43. Pazdro, R., Burgess, J.R. (2010). The role of vitamin E and oxidative stress in diabetes complications. *Mechanism of Ageing and Development, 131(4):276-86.*

44. Penn, J.S., Thum, L.A., Rhem, M.N., Dell, S.J. (1988). Effects of oxygen rearing on the electroretinogram and GFA-protein in the rat. *Investigative Ophthalmology & Visual Science,* 29(11):1623-30.

45. Pickard, G.E., Baver, S.B., Ogilvie, M.D., Sollars, P.J. (2009). Light-Induced Fos Expression in Intrinsically Photosensitive Retinal Ganglion Cells in Melanopsin Knockout (Opn42/2) Mice. *PLoS One*, 4(3):e4984.

46. Razjouyan, J., Gharibzadeh, S., Ali Fallah, A. (2009). Organizational Role of Retina Horizontal Cells. The *Journal of Neuropsychiatry and Clinical Neuroscience*, 21(4):479-80.

47. Richard, H.M. (2001).The fundamental plan of the retina. *Nature Neuroscience,* 4(9): 877-86.

48. Riva, C.E., Grunwold, J.E., Perrig, D.L. (1983). Reactivity of the Human Retinal Circulation to Darkness: A Laser Doppler Velocimetry Study. *Investigative Ophthalmology and Visual Science,* 24(6):737-40.

49. Salminen, A., Kauppinen, A., Hyttinen, J.M., Toropainen, E., Kaarniranta, K. (July 2010). Endoplasmic reticulum stress in age-related macular degeneration (AMD): trigger for neovascularization. *Molecular Medicine.* Repéré à: http://www.molmed.org

50. Saszik, S., Bilotta, J. (2001). Constant dark-rearing effects on visual adaptation of the zebrafish ERG. *International Journal of Developmental Neuroscience,* 19(7):611-9.

51. Sernagor, E. (2005). Retinal Development: Second Sight Comes First. *Current Biology*, 15(14): R556-9.

52. Simó, R., Villarroel, M., Corraliza, L., Hernández, C., Garcia-Ramírez, M. (2010). The Retinal Pigment Epithelium: Something More then a Constituent of the Blood-Retinal Barrier—Implications for the Pathogenesis of Diabetic Retinopathy. *Journal of Biomedicine & Biotechnology*, 2010:190724.

53. Stockton, R.A., Slaughter, M.M. (1989). B-wave of the electroretinogram. A reflection of ON bipolar cell activity. *The Journal of General Physiology,* 93(1):101-22.

54. Strauss, O. (2005). The Retinal Pigment Epithelium in Visual Function. *Physiological Review,* 85(3):845-81

55. Tam, B.M., Moritz, O.L. (2007). Dark Rearing Rescues P23H Rhodopsin-Induced Retinal Degeneration in a Transgenic Xenopus laevis Model of Retinitis Pigmentosa: A Chromophore-Dependent Mechanism Characterized by Production of N-Terminally Truncated Mutant Rhodopsin. *The Journal of Neuroscience,* 27(34):9043-53.

56. Terrasa, A.M., Guajardo, M.H., Marra, C.A., Zapata, G. (2009). Alpha-tocopherol protects against oxidative damage to lipids of the rod outer segments of the equine retina. *Veterinary Journal,* 82(3):463-8.

57. Toga, A.W. (1987). The metabolic consequence of visual deprivation in the rat. *Brain Research,* 465(1-2): 209-17.

58. Vigh, J., Banvolgyi, T., Wilhelms, M. (2000). Amacrine Cells of the Anuran Retina: Morphology, Chemical Neuroanatomy, and Physiology. *Microscopy Research and Technique*, 50(5):373-83.

59. Villegas, G.M. (1960). Electron Microscopic Study of the Vertebrate Retina. *The Journal of General Physiology,* 43(6)Suppl: 15-43.

60. Wachtmeister, L., Dowling, J.E. (1978). The oscillatory potentials of the mudpuppy retina. *Investigative Ophthalmology and Visual Science,* 17(12):1176-88.

61. Wang, L., Kondo, M., Bill, A. (1997). Glucose Metabolism in Cat Outer Retina Effects of Light and Hyperoxia. *Investigative Ophthalmology and Visual Science,* 38(1):48-55.

62. Wasle, H., Boycott B.B. (1991). Functional Architecture of the Mammalian Retina. *Physiological Reviews,* 71(2): 447-80.

63. Wen, R., Oakley, B. (1990). K(+)-evoked Müller cell depolarization generates b-wave of electroretinogram in toad retina. *Procreedings of the National Academy of Science of the United States of America,* 87(6):2117-21.

64. Yanagida, T., Tomita, T. (1982). Local potassium concentration changes in the retina and the electroretinographic (ERG) b-wave. *Brain Research,* 237(2):479-83.

65. Zhiyin Liang, Z., Freed, M.A. (2010). The ON Pathway Rectifies the OFF Pathway of the Mammalian Retina. *The Journal of Neuroscience,* 30(16):5533-43.

Manuel

66. Kandel, E.R., Schwartz, J.H., Jessell, T.M. (2000). *Principles of neural science*. New York, NY: McGraw-Hill, Health Professions Division.

Other

67. Faber, D. S. (1969). *Analysis of the slow transretinal potentials in response to light* (Ph.D. Thesis). State University of New York, Buffalo.

6 CAPTIONS TO TABLES AND FIGURES

- **Figure 4:** Representative scotopic (mixed rod-cone, flash intensity: -6.3 through 0.9 log cd.s/m^{-2}) ERGs obtained at P30. Four groups are represented: normoxic (21% O_2) rats raised in normal (80 lux.) light environment (NC group), normoxic rats dark reared from P0 to P14 (DR14 group), normoxic rats dark reared from P0 to P28 (DR28 group) and dark reared (P0-P14) rats exposed to hyperoxia (80% O_2) from P0 to P14 (DRO_2 group). Calibrations: horizontal, 20 ms, vertical 1000 µV.

- **Figure 5:** Graphic representation of a-wave (top) and b-wave (bottom) amplitudes fitted to sigmoidal luminance dose-response function curves. Progressively brighter stimuli evoke higher amplitudes of scotopic a- and b-waves. The amplitudes of scotopic a- and b-waves obtained at P30 are ordinate in micro volts. As shown in the legend, different groups are represented by different colour lines. The results are presented as the mean amplitude ± standard deviation (SD).

- **Figure 6:** Graphic representation of the mean values of a-wave (top) and b-wave (bottom) amplitudes (in micro volts) evoked by the highest (0.9 log cd.s/m^{-2}) flash intensity. The results were obtained at P30. Four groups are compared each represented by different colour: NC group (red), DR14 group (black), DR28 group (green) and DRO_2 group (blue). A one-way ANOVA and Tukey tests comparing each group data were

used in order to detect statistically significant ($P < 0.05$) differences between regiments. $*^{+x}$ represent significant differences from the colour-corresponding group. The results are presented as the mean values ± standard deviation (SD).

- **Figure 7:** Graphic representation of the mean values of the rod Vmax (maximum rod response without cone contamination) obtained at P30. As shown in the legend, different groups are represented by different colour. A one-way ANOVA and Tukey tests comparing different group data were used to detect significant ($P < 0.05$) differences between each cohort. $*^{+x}$ represent significant differences from the colour-corresponding group. The results are presented as the mean values ± standard deviation (SD).

- **Figure 8a-(top):** Representative photopic (flash intensity: 0.9 log $cd.s/m^{-2}$, background: 30 $cd.m^{-2}$) ERGs obtained at P30. Each group is represented by different colour: NC group (red), DR14 group (black), DR28 group (green) and DRO_2 group (blue). Photopic ERGs for each group were recorded 5, 10, 15 and 20 min. following adaptation to the background light. Calibrations: horizontal, 20 ms and vertical, 200 µV. **8b-(bottom):** Graphic representation of the mean values of the photopic b-wave amplitudes obtained at different time points following the background light adaptation. A one-way ANOVA and Tukey tests comparing different group data were used to detect significant ($P <$

0.05) differences between each cohort. $^{*+x\,o}$ represent significant differences from the colour-corresponding group. The results are presented as the mean values ± standard deviation (SD). The legend explains the colour differentiation of each group.

- **Figure 9:** Representative scotopic (mixed rod-cone, flash intensity: -6.3 through 0.9 log cd.s/m-2) ERGs obtained at P60. Dark reared from P0 to P14 SD rat pups were exposed to hyperoxia for the same period (DRO2 group) Further, they were compared to normal pups that were dark reared from P0 to P14 (DR14 group) or from P0-to P28 (DR28 group). All dark reared groups were compared to age matched pups raised in normal light conditions (NC group). Calibrations: horizontal, 20 ms, vertical 1000 µV.

- **Figure 10:** Graphic representation of a-wave (top) and b-wave (bottom) amplitudes fitted to sigmoidal luminance dose-response function curves. Progressively brighter stimuli evoke higher amplitudes of scotopic a- and b-waves. The amplitudes of scotopic a- and b-waves obtained at P60 are ordinate in micro volts. Four compared groups are represented by different colour lines: NC group (red), DR14 group (black), DR28 group (green) and DRO_2 group (blue). The results are presented as the mean amplitude ± standard deviation (SD).

- **Figure 11:** Graphic representation of the mean values of a-wave (top) and b-wave (bottom) amplitudes (in micro volts) evoked by the highest (0.9 log cd.s/m^{-2}) flash intensity. The results were obtained at P30. As shown at legend, four groups are compared each represented by different colour. A one-way ANOVA and Tukey tests comparing each group data were used in order to detect statistically significant ($P < 0.05$) differences between regiments. $*^{+x\,o}$ represent significant differences from the colour-corresponding group. The results are presented as the mean values ± standard deviation (SD).

- **Figure 12:** Graphic representation of the mean values of the rod Vmax (maximum rod response without cone contamination) obtained at P60. Four groups compared in this figure are represented by different colour. A one-way ANOVA and Tukey tests comparing different group data were used to detect significant ($P < 0.05$) differences between each cohort. $*^{+xo}$ represent significant differences from the colour-corresponding group. The results are presented as the mean values ± standard deviation (SD).

- **Figure 13a-(top):** Representative photopic (flash intensity: 0.9 log cd.s/m^{-2}, background: 30 cd.m^{-2}) ERGs obtained at P60. Each group is represented by different colour: NC group (red), DR14 group (black), DR28 group (green) and DRO_2 group (blue). Photopic ERGs for each

group were recorded 5, 10, 15 and 20 min. following adaptation to the background light. Calibrations: horizontal, 20 ms and vertical, 200 µV. **13b-(bottom):** Graphic representation of the mean values of the photopic b-wave amplitudes obtained at different time points following the background light adaptation. A one-way ANOVA and Tukey tests comparing different group data were used to detect significant ($P < 0.05$) differences between each cohort. $^{*+x\,o}$ represent significant differences compared to the colour-corresponding group. The results are presented as the mean values ± SD.

- **Figure 14:** Graphic representation of the mean thickness of different retinal layers (in micrometers) in dark reared animals raised in hyperoxic (DRO_2) or normoxic (DR14, DR28) environements and compared with normoxic rats raised in normal light environment. Mesurements were obtained at postnatal day P30. $^{*+x\,o}$ Statistically significant ($P < 0.05$) differences were found using a one-way ANOVA and Tukey tests. The results are given as the mean thickness ± SD.

- **Figure 15:** Representative retinal histological sections (superior retina 1000 µm from optic nerve head) obtained at P30. NC, DR14, DR28 and DRO_2 groups are represented by red, black, green and blue colour respectively. RPE, retinal pigment epithelium layer; OS, outer photoreceptor layer; IS, inner photoreceptor layer; ONL, outer nuclear layer; OPL, outer plexiform layer; INL, inner nuclear layer; IPL, inner

plexiform layer and GCL, ganglion cell layer are shown. Magnification: x40; scale: 50 µm.

- **Figure 16:** Graphic representation of the mean thickness of different retinal layers (in micrometers) in dark reared animals raised in hyperoxic (DRO_2) or normoxic (DR14, DR28) environements and compared with normoxic rats raised in normal light environment. Measurements were obtained at P60. $*^{+x\,o}$ represent statistically significant ($P < 0.05$) differences found using a one-way ANOVA and Tukey tests. The results are given as the mean thickness ± SD.

- **Figure 17:** Representative retinal histological sections (superior retina 1000 µm from optic nerve head) obtained at P60. Each group is represented by different colour: NC group (red), DR14 group (black), DR28 group (green) and DRO_2 group (blue). Different retinal layers are represented by corresponding abbreviations. Magnification: x40; scale: 50 µm.

- **Figure 18:** Representative scotopic (mixed rod-cone, flash intensity: -6.3 through 0.9 log $cd.s/m^{-2}$) ERGs obtained at P30. SD albino rats were intravitreously injected either with paraquat at postnatal day P7, P14 and P21 (paraquat treated groups are named accordingly to the day of injections) or with PBS (Control group). Despite amplification

(10x) of waveforms obtained in P7 group (dashed frame) we were not able to record any functional activity in this particular group. Calibrations: horizontal, 20 ms, vertical 1000 µV.

- **Figure 19:** Graphic representation of a-wave amplitudes fitted to sigmoidal luminance dose-response function curves. Progressively brighter stimuli evoke higher amplitudes of scotopic a-waves. The amplitudes of scotopic a-waves obtained at P30, P45 and P60 are ordinate in micro volts. As shown in the legend, different groups are represented by different colour lines: Control group in red, P7 group in black, P14 group in green and P21 group in blue. * Compared to the Control group statistically significant ($P < 0.05$) differences found using a one-way ANOVA and Tukey tests. The results are presented as the mean amplitude ± standard deviation (SD).

- **Figure 20:** Graphic representation of b-wave amplitudes fitted to sigmoidal luminance dose-response function curves. Progressively brighter stimuli evoke higher amplitudes of scotopic a-waves. The amplitudes of scotopic b-waves obtained at P30, P45, P60 are ordinate in micro volts. Different groups are represented by different colour lines. * Compared to the Control group statistically significant ($P < 0.05$) differences obtained using a one-way ANOVA and Tukey tests. The results are presented as the mean amplitude ± standard deviation (SD).

- **Figure 21:** Graphic representation of the mean values of the rod Vmax (maximum rod response without cone contamination) obtained at P30, P45 and P60. Different experimental groups are represented by different colour. A one-way ANOVA and Tukey tests comparing different group data were used to detect significant ($P < 0.05$) differences between each cohort. * Significantly different from the Control group. The results are presented as the mean values ± standard deviation (SD).

- **Figure 22:** Representative scotopic (mixed rod-cone, flash intensity: -6.3 through 0.9 log cd.s/m^{-2}) ERGs obtained at P45. SD albino rats intravitreously injected with paraquat at postnatal day P7 (P7 group), P14(P14 group) and P21 (P21 group) are compared with PBS injected Control group. Calibrations: horizontal, 20 ms, vertical 1000 μV.

- **Figure 23:** Representative scotopic (mixed rod-cone, flash intensity: -6.3 through 0.9 log cd.s/m^{-2}) ERGs obtained at P60. Paraquat injected SD rats are compared to the Control group. Calibrations: horizontal, 20 ms, vertical 1000 μV.

- **Figure 24:** Graphic representation of a-wave (left) and b-wave (right) amplitudes fitted to sigmoidal luminance dose-response function curves. The amplitudes of scotopic a- and b-vaves obtained at P30,

P45 and P60 are ordinate in micro volts. Each time point when the recordings were done are presented in different colour: P30 in black, P45 in green and P60 in bleu.

- **Figure 25a-(top):** Representative photopic (flash intensity: 0.9 log cd.s/m^{-2}, background: 30 cd.m^{-2}) ERGs obtained at P30. Each group is represented by different colour: Control group (red), P7 group (black), P14 group (green) and P21 group (blue). Photopic ERGs for each group were recorded 5, 10, 15 and 20 min. following adaptation to the background light. Calibrations: horizontal, 20 ms and vertical, 200 µV. **25b-(bottom):** Graphic representation of the mean values of the photopic b-wave amplitudes obtained at different time points following the background light adaptation. A one-way ANOVA and Tukey tests comparing different group data were used to detect significant ($P < 0.05$) differences between each cohort. * Significantly different from the Control group. The results are presented as the mean values ± SD.

- **Figure 26a-(top):** Representative photopic (flash intensity: 0.9 log cd.s/m^{-2}, background: 30 cd.m^{-2}) ERGs obtained at P45. Each group is represented by different colour. Photopic ERGs for each group were recorded 5, 10, 15 and 20 min. following adaptation to the background light. Calibrations: horizontal, 20 ms and vertical, 200 µV. **26b-(bottom):** Graphic representation of the mean values of the photopic b-wave amplitudes obtained at different time points following the

background light adaptation. A one-way ANOVA and Tukey tests comparing different group data were used to detect significant ($P < 0.05$) differences between each cohort. * Significantly different from the Control group. The results are presented as the mean values ± SD.

- **Figure 27a-(top):** Representative photopic (flash intensity: 0.9 log cd.s/m^{-2}, background: 30 cd.m^{-2}) ERGs obtained at P60. Each group is represented by different colour. Photopic ERGs for each group were recorded 5, 10, 15 and 20 min. following adaptation to the background light. Calibrations: horizontal, 20 ms and vertical, 200 µV. **27b-(bottom):** Graphic representation of the mean values of the photopic b-wave amplitudes obtained at different time points following the background light adaptation. A one-way ANOVA and Tukey tests comparing different group data were used to detect significant ($P < 0.05$) differences between each cohort. * Significantly different from the Control group. The results are presented as the mean values ± SD.

- **Figure 28:** Graphic representation of the mean values of rod V_{max} (left) and photopic b-wave (right) amplitudes recorded at different time points. Time dependant amplitude fluctuations within the same group are ordinate in micro volts. Each time point when the recordings were done is presented in different colour: P30 in black, P45 in green and P60 in bleu.

- **Figure 29a-(left):** Representative retinal histological sections (central retina) obtained at post natal days P30, P45 and P60. Each group is represented by different colour: Control group (red), P7 group (black), P14 group (green) and P21 group (blue). Magnification: x40; scale: 50 µm. **29b-(right):** folding in ONL observed in P21 group at postnatal day P30 (9 days following paraquat injection).

- **Table 1:** Group data comparing the amplitude measurements of all ERG parameters (scotopic a- and b-wave, rod Vmax and photopic b-wave) obtained from NC and DR28 groups at postnatal day P30 and P60. The results are presented as the mean values ± SD.

- **Table 2:** Group data comparing the amplitude measurements of all ERG parameters (scotopic a- and b-wave, rod Vmax and photopic b-wave) obtained from SD rats exposed to hyperoxia from postnatal day P0 to P14, and age matched dark reared SD rats exposed to hyperoxia for the same period. * illustrate the results obtained in our laboratory by Dorfman et al. (2009). The results are presented as the mean values ± SD.

- **Table 3:** Group data comparing the amplitude measurements of all ERG parameters (scotopic a- and b-wave, rod Vmax and photopic b-wave) obtained from paraquat treated SD rats (P7, P14, P21) and

control cohort (Control). The results were obtained at postnatal days P30, P45 and P60. The results are presented as the mean values ± SD.

- **Table 4:** Group data comparing the mean thickness (± SD) of the ONL obtained from paraquat treated SD rats (P7, P14, P21) and control cohort (Control). The results were obtained at postnatal days P30, P45 and P60.

7 FIGURES

Figure 4: Representative scotopic mixed rod-cone ERG waveforms (P30)

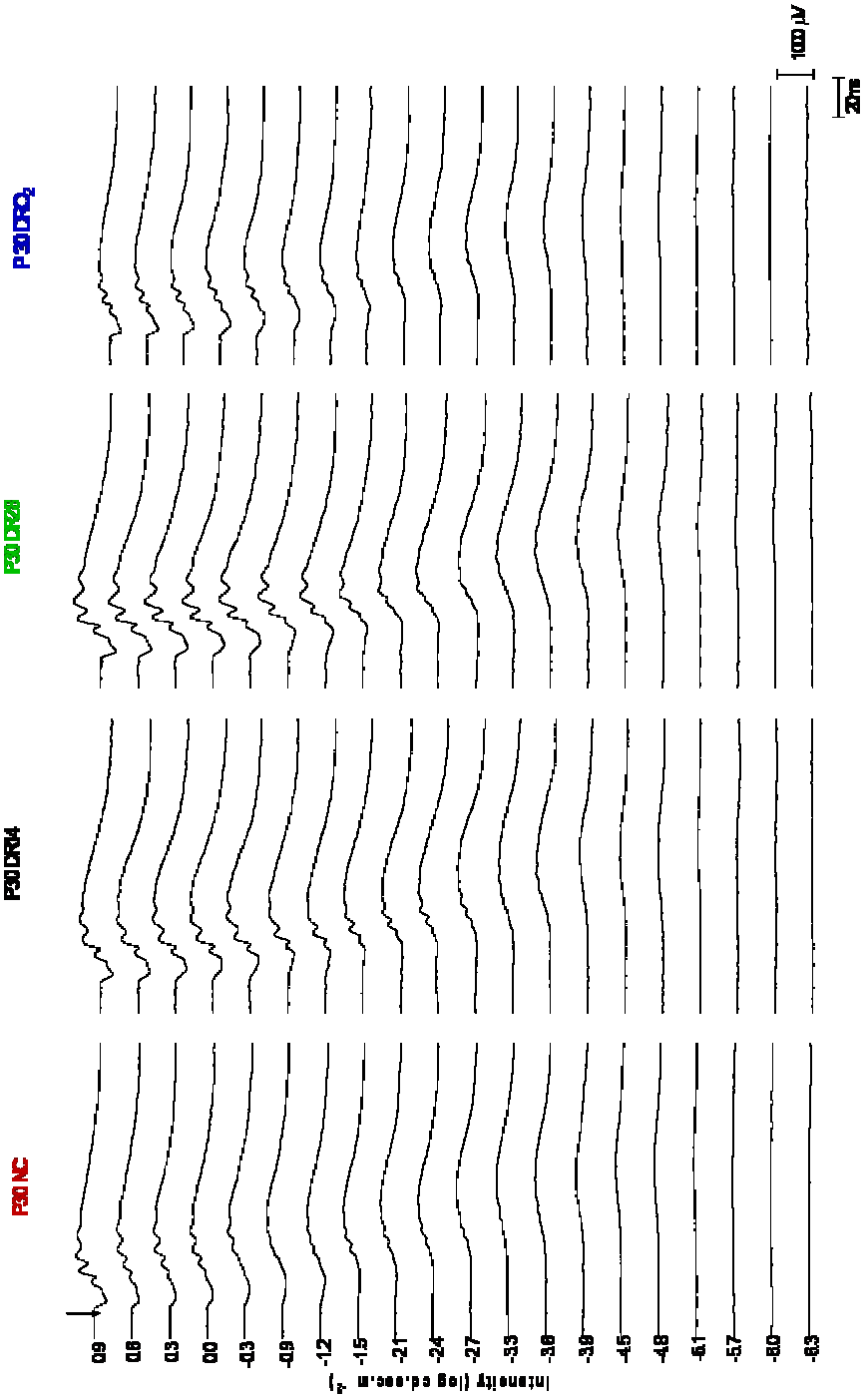

Figure 5: Graphic representation of a-wave (top) and b-wave (bottom) luminance dose-response curves (P30)

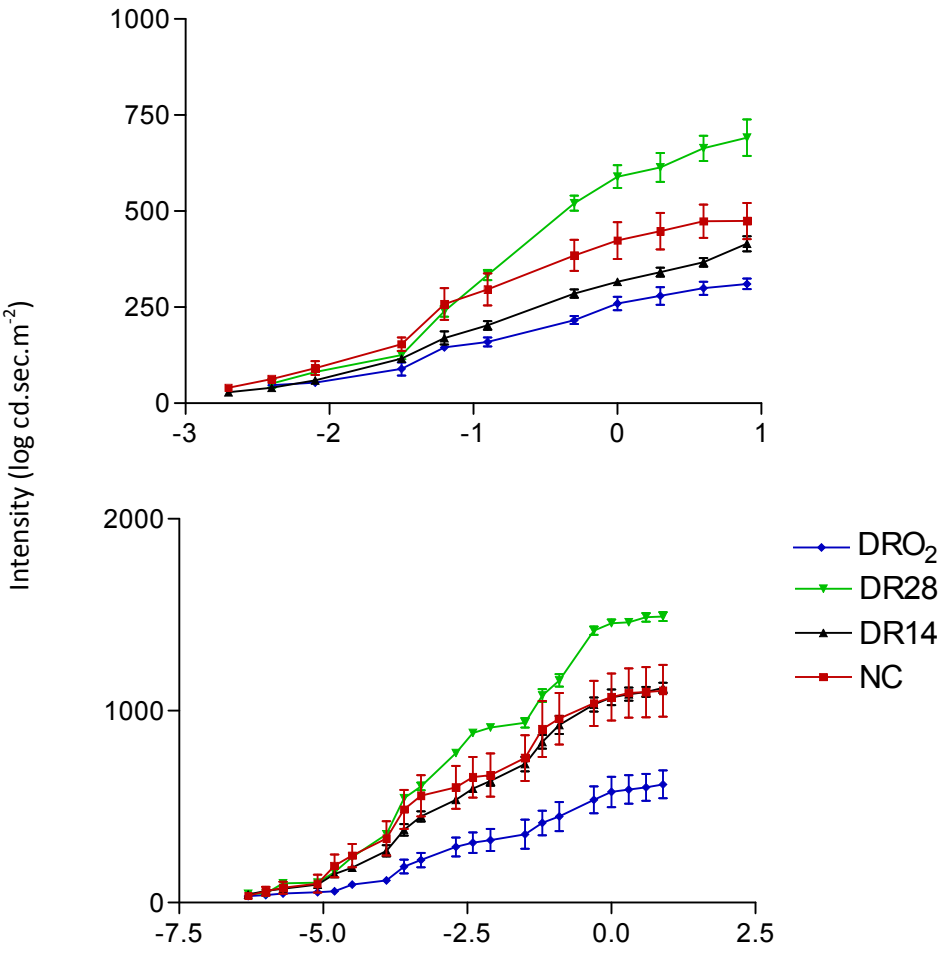

Figure 6: Graphic representation of the mean values of a-wave (top) and b-wave (bottom) amplitudes (P30)

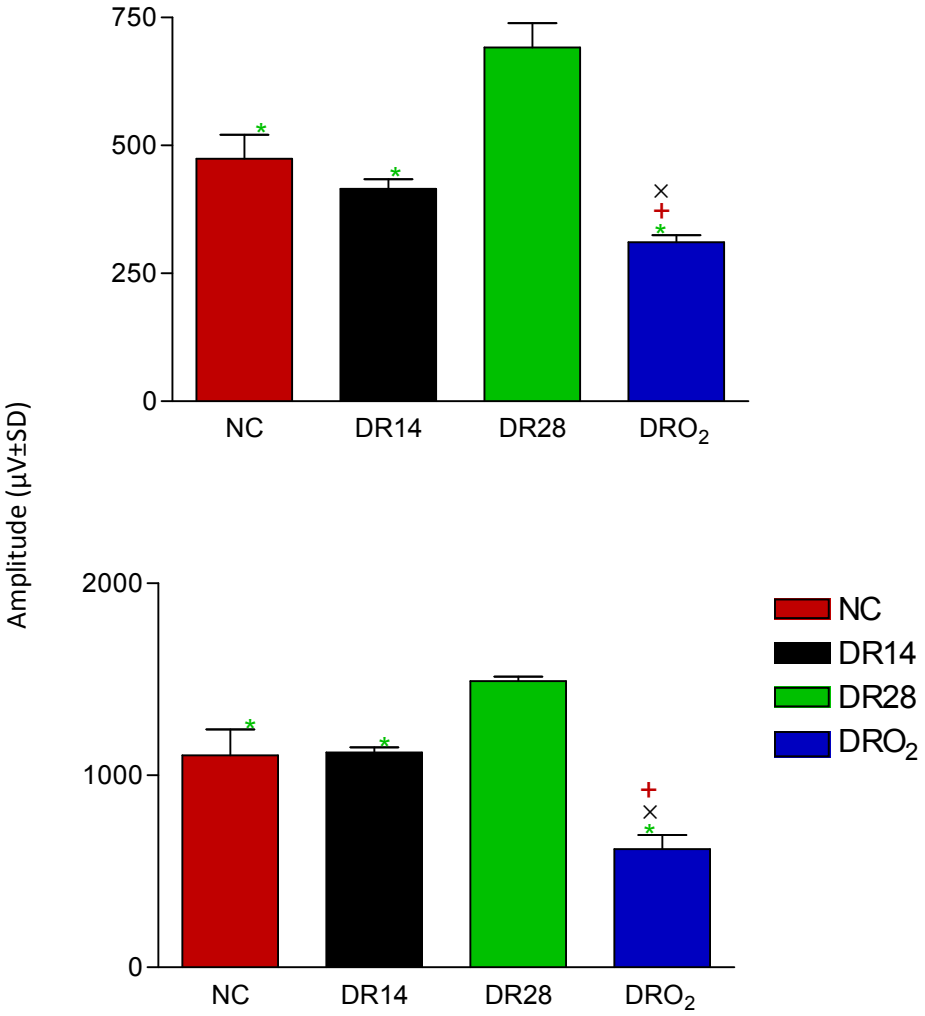

Figure 7: Graphic representation of the mean values of the rod Vmax (P30)

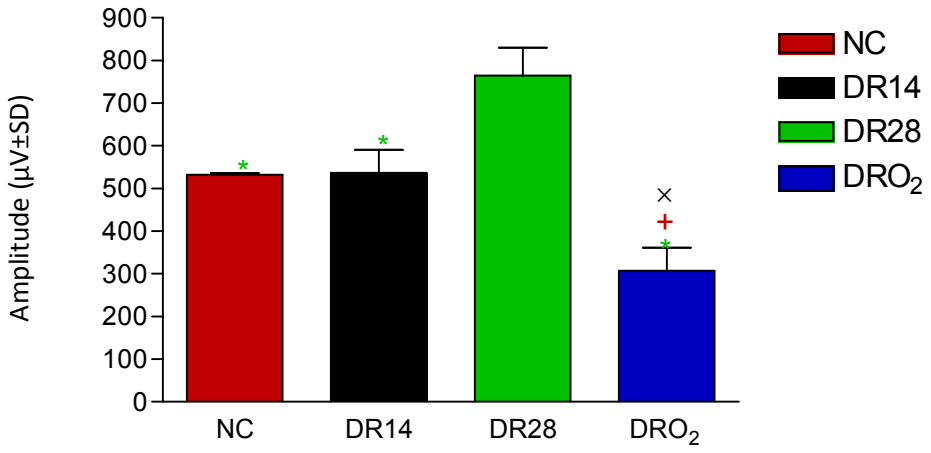

Figure 8: Representative photopic ERG waveforms (top), graphic representation of the mean values of the photopic b-wave amplitudes (bottom) (P30)

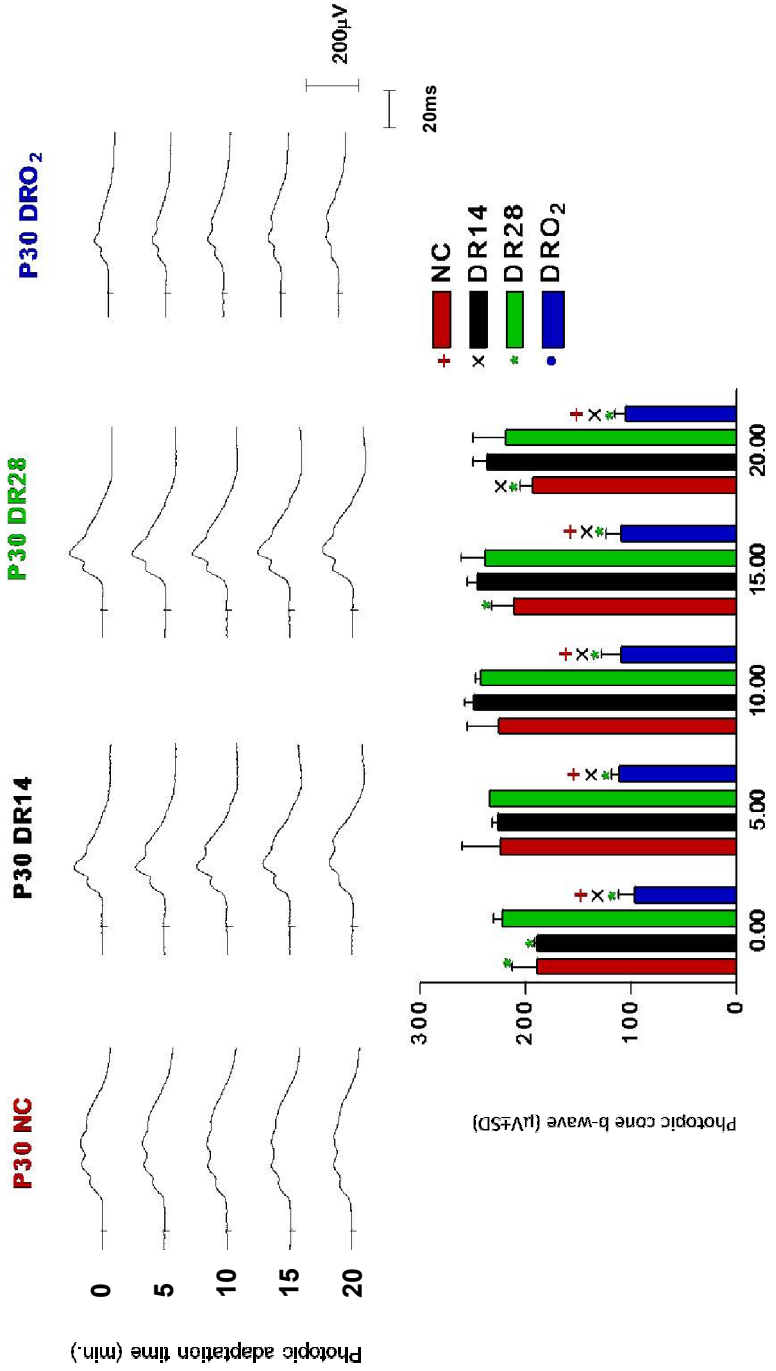

Figure 9: Representative scotopic mixed rod-cone ERG waveforms (P60)

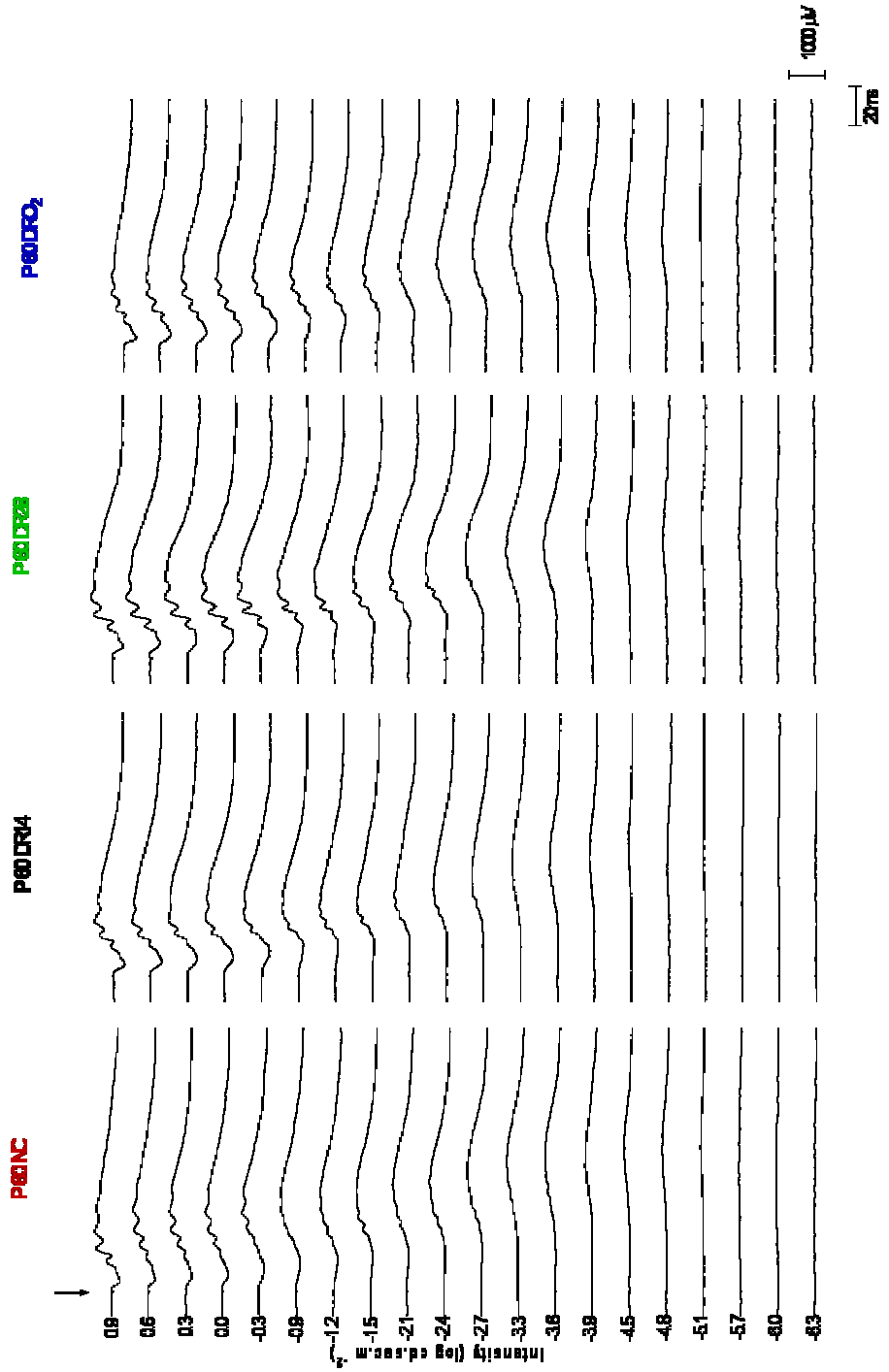

Figure 10: Graphic representation of a-wave (top) and b-wave (bottom) luminance dose-response curves (P60)

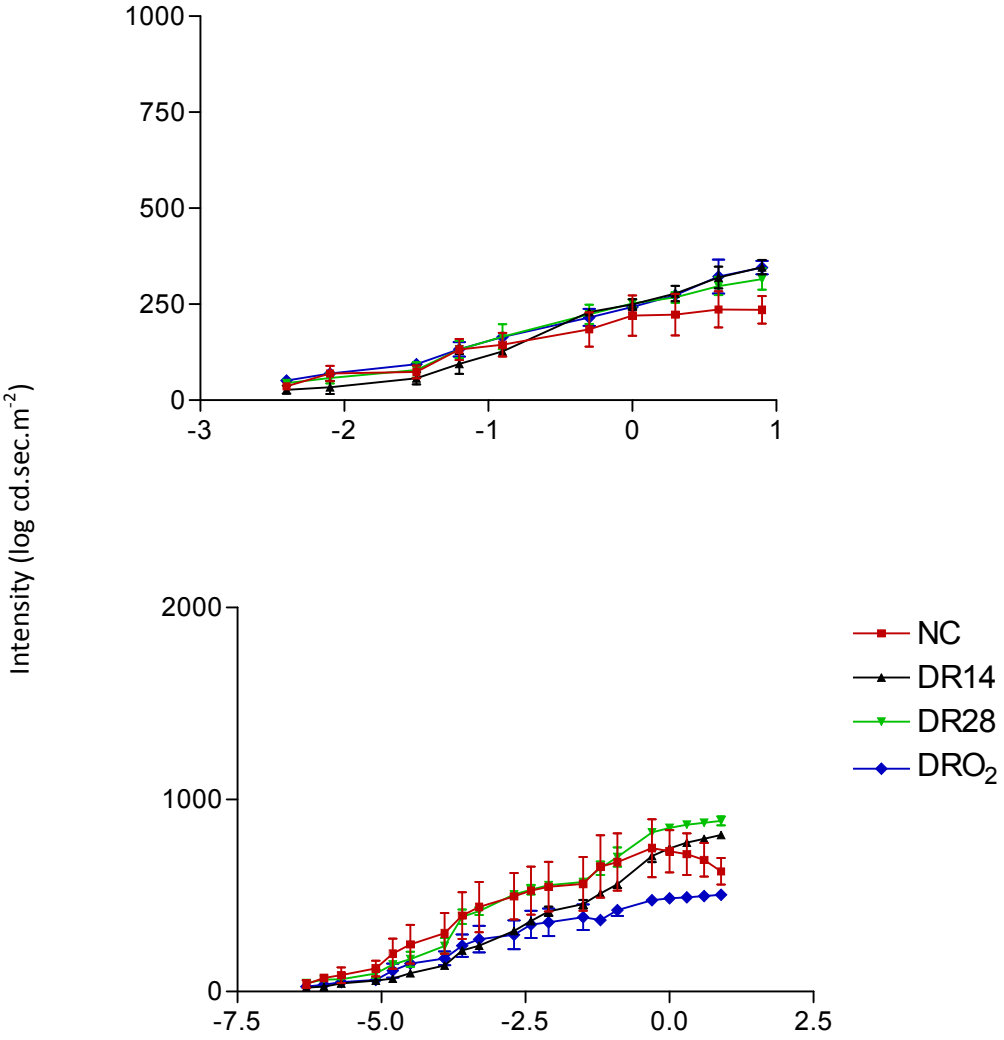

Figure 11: Graphic representation of the mean values of a-wave (top) and b-wave (bottom) amplitudes (P60)

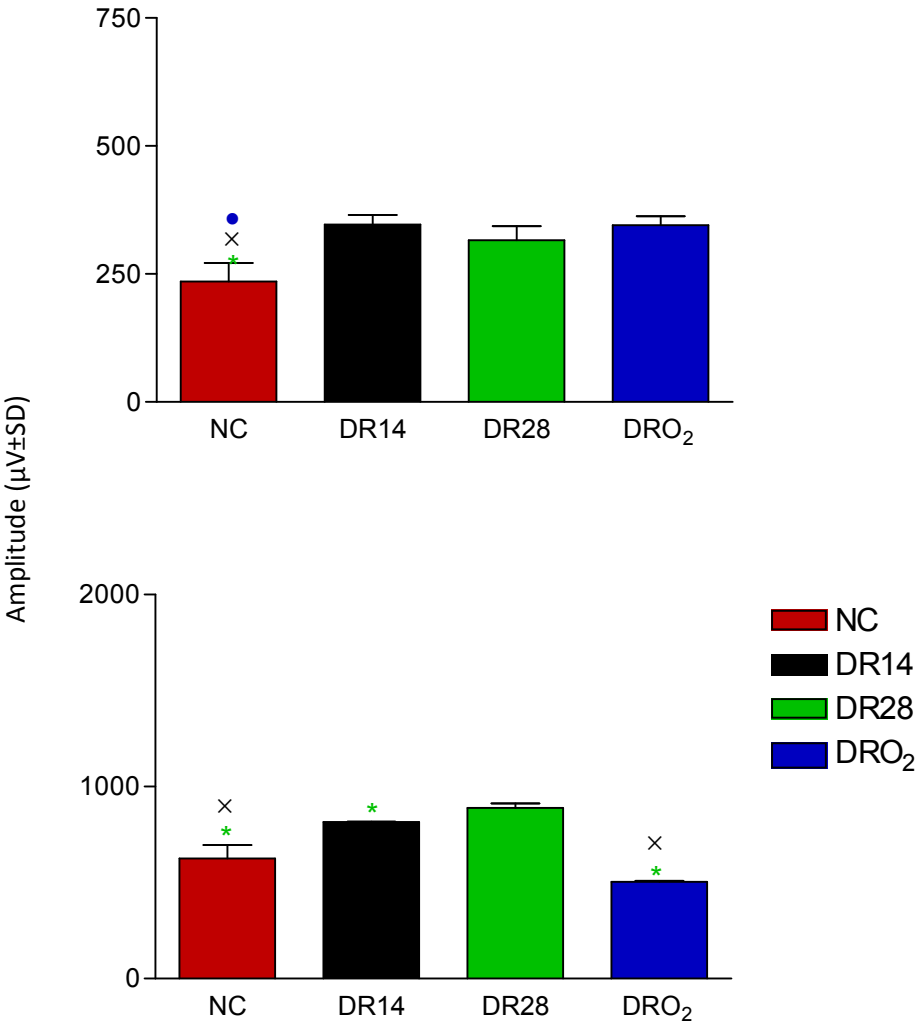

Figure 12: Graphic representation of the mean values of the rod Vmax (P60)

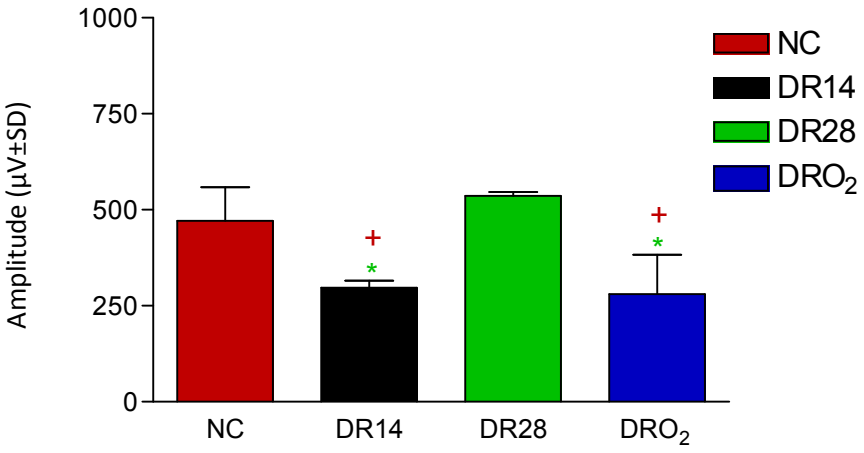

Figure 13: Representative photopic ERG waveforms (top), graphic representation of the mean values of the photopic b-wave amplitudes (bottom) (P60)

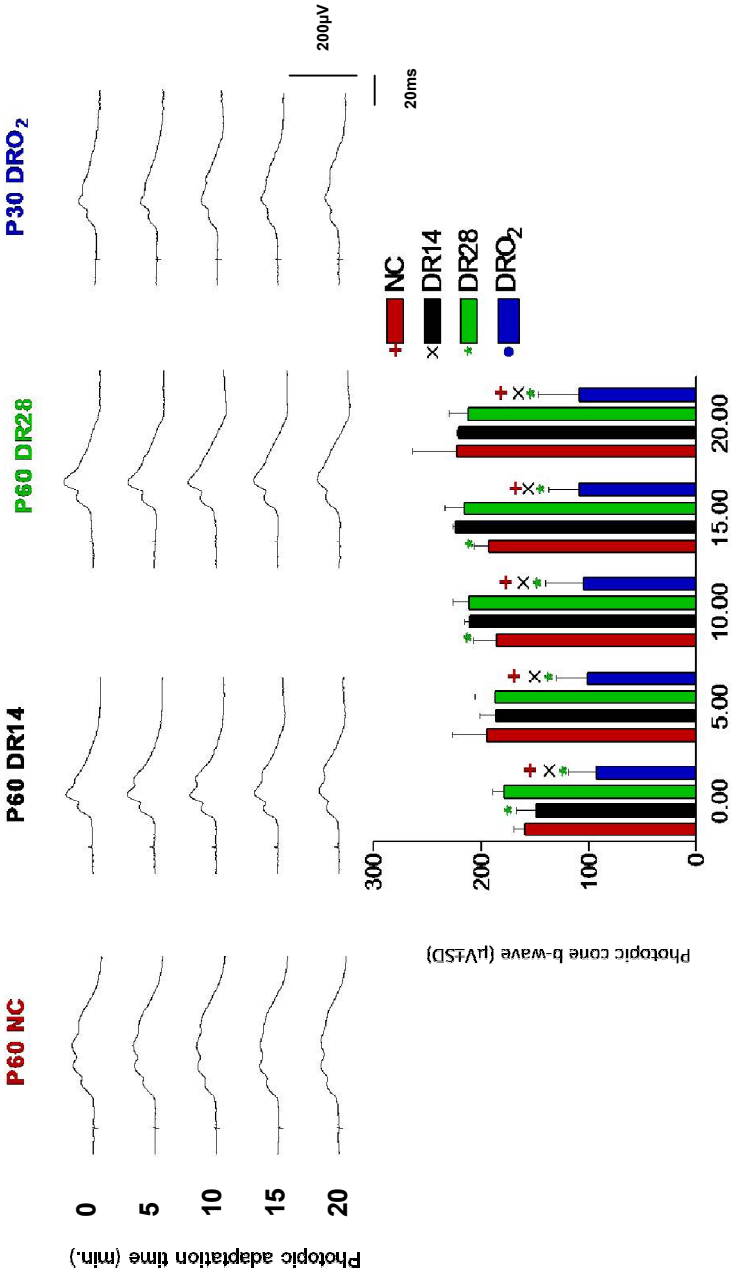

Figure 14: Graphic representation of the mean thickness of different retinal layers (P30)

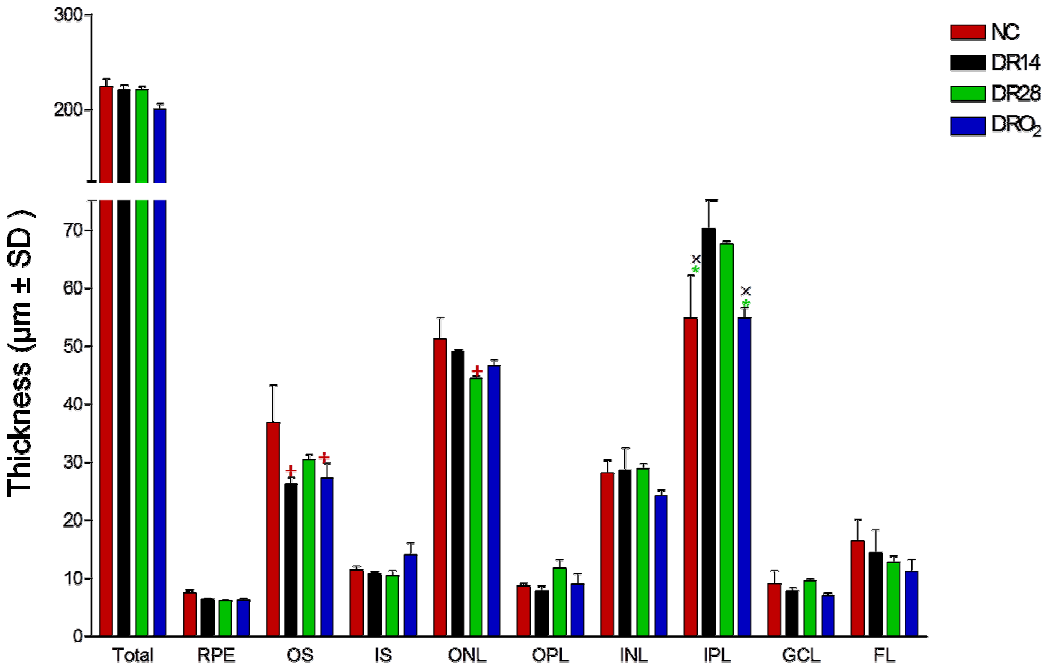

Figure 15: Representative retinal histological sections (P30)

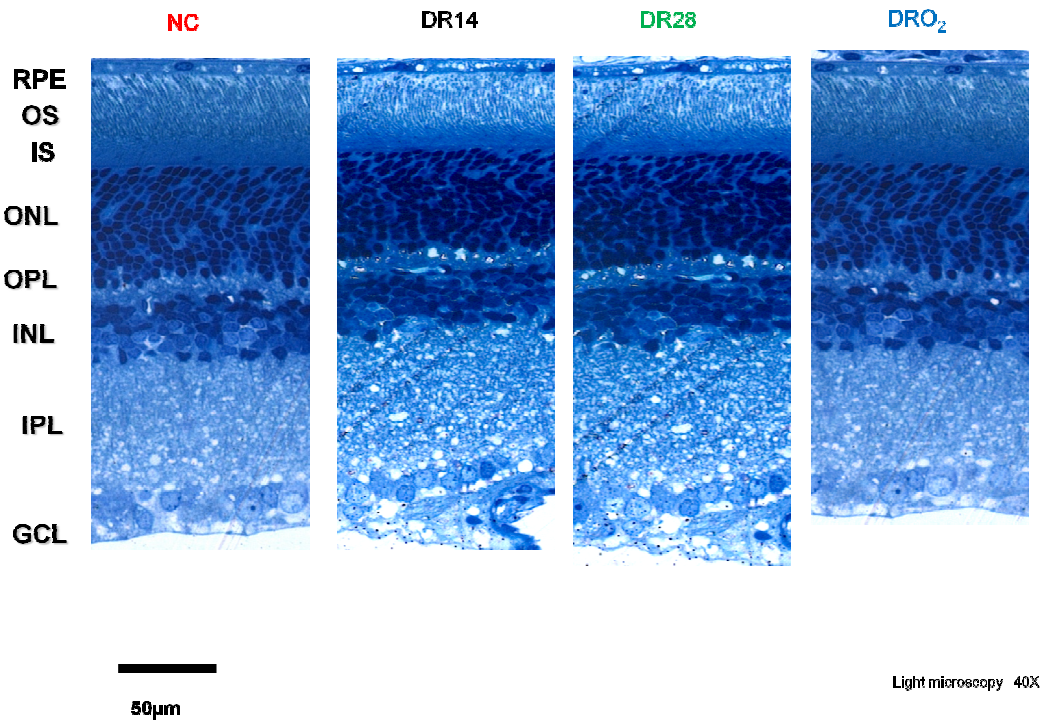

Figure 16: Graphic representation of the mean thickness of different retinal layers (P60)

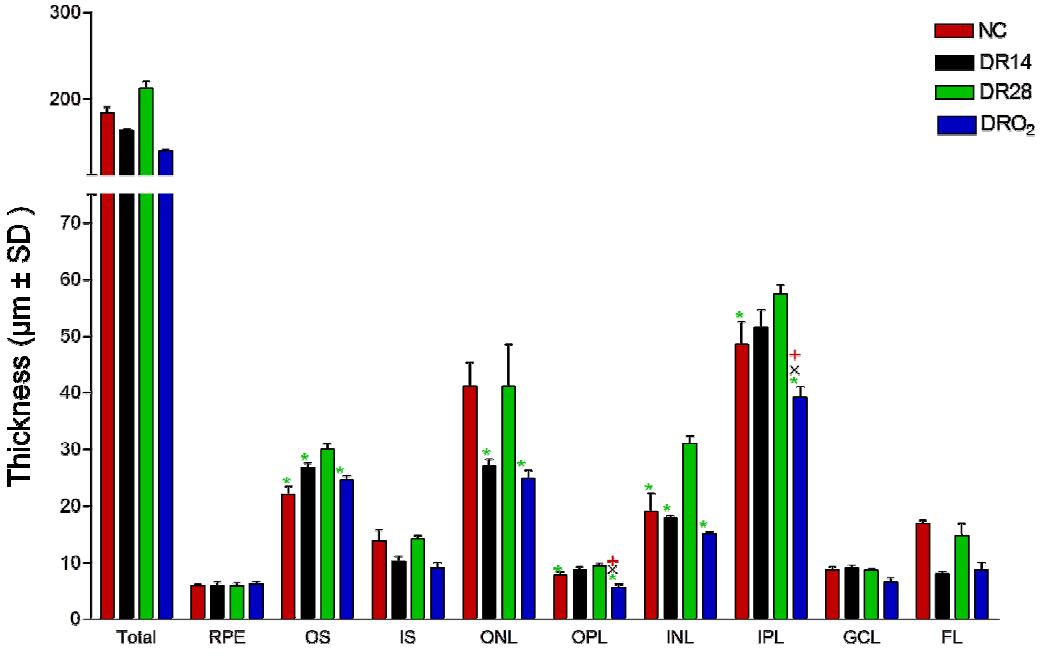

Figure 17: Representative retinal histological sections (P60)

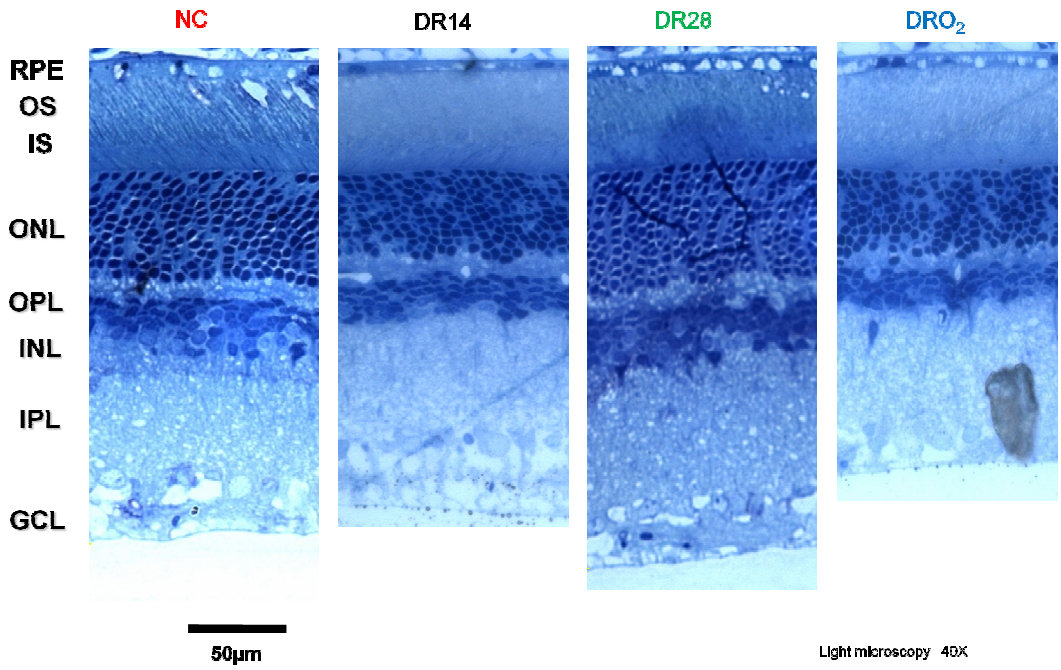

Figure 18: Representative scotopic mixed rod-cone ERG waveforms (P30)

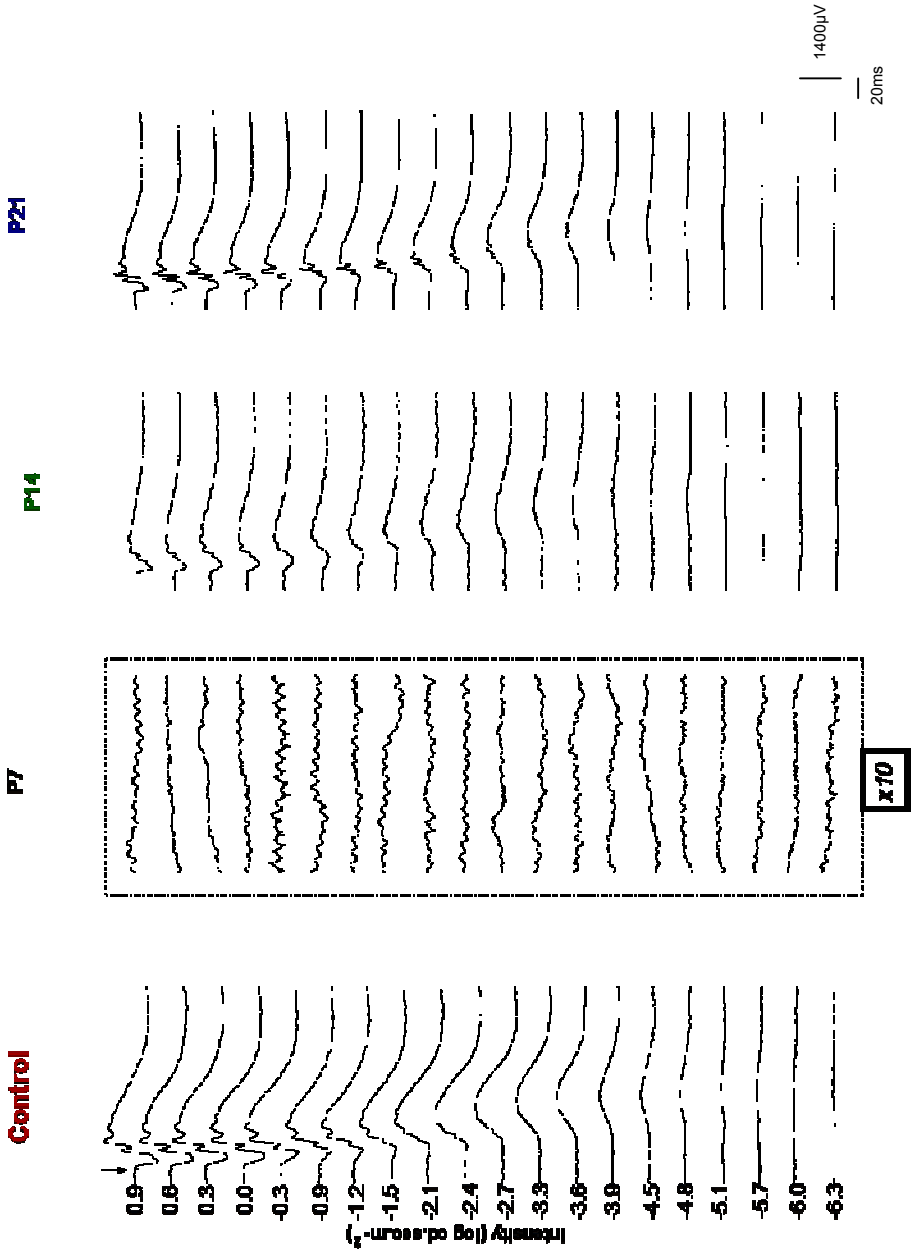

Figure 19: Graphic representation of a-wave luminance dose-response curves (P30, P45, P60)

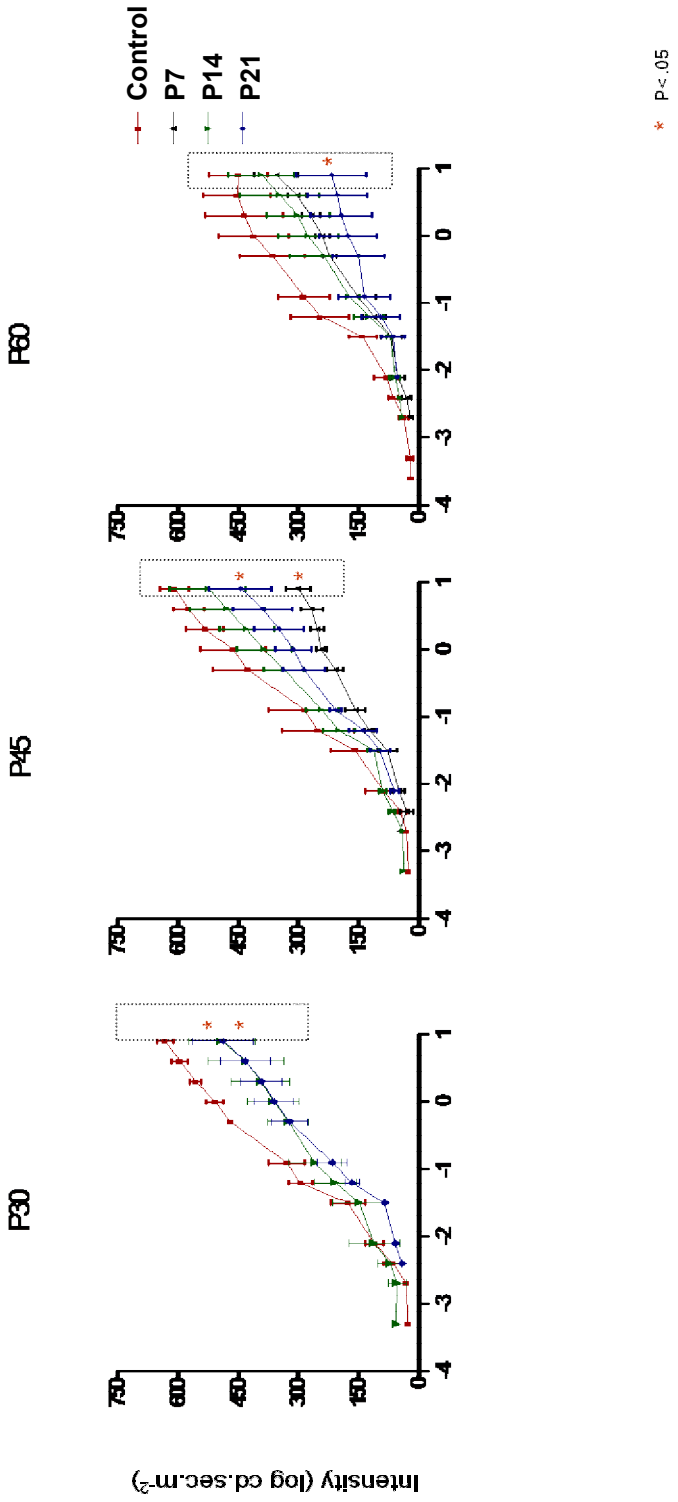

Figure 20: Graphic representation of b-wave luminance dose-response curves (P30, P45, P60)

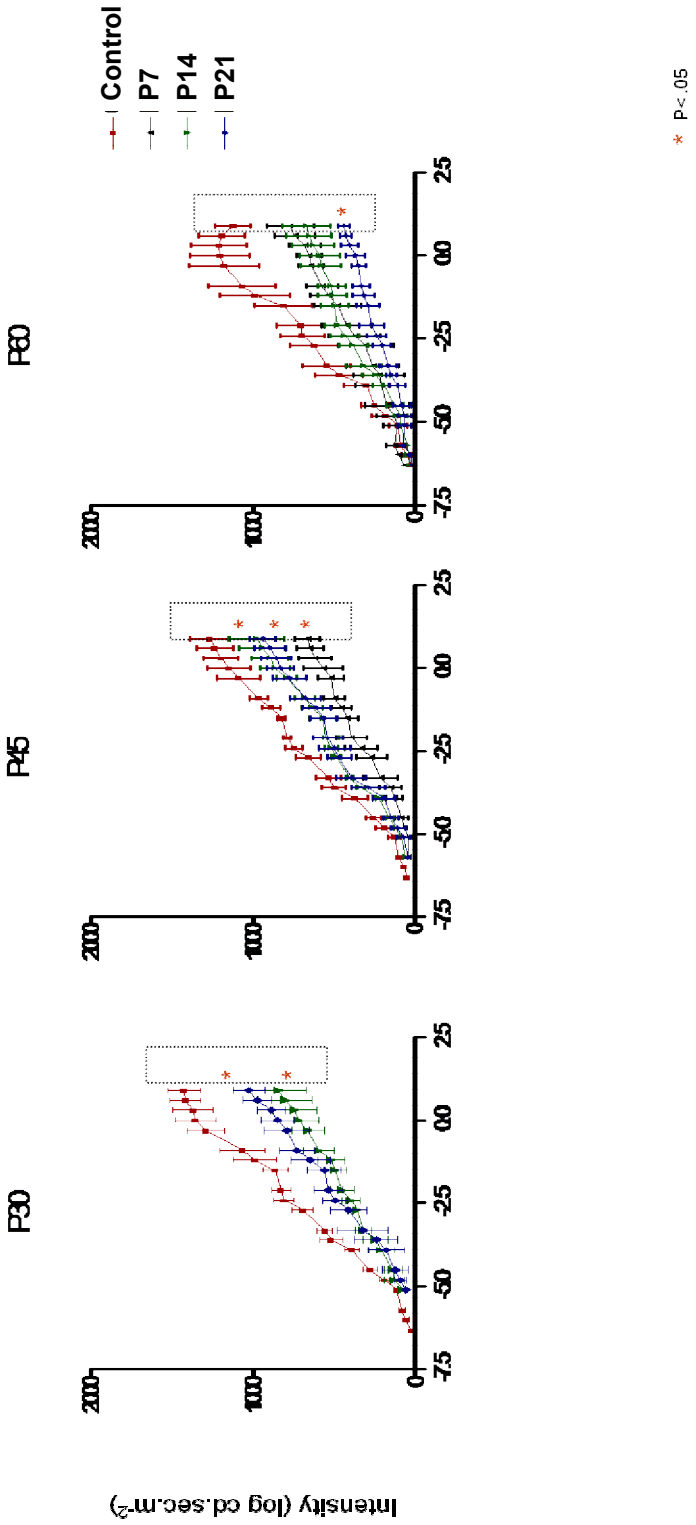

Figure 21: Graphic representation of the mean values of the rod Vmax (P30, P45, P60)

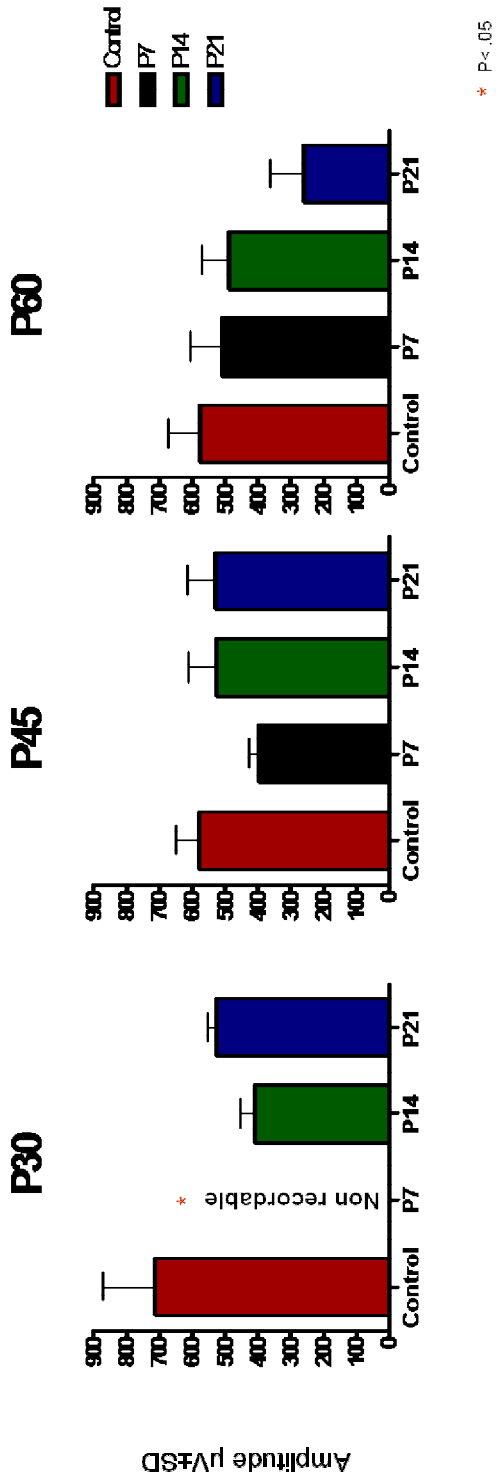

Figure 22: Representative scotopic mixed rod-cone ERG waveforms (P45)

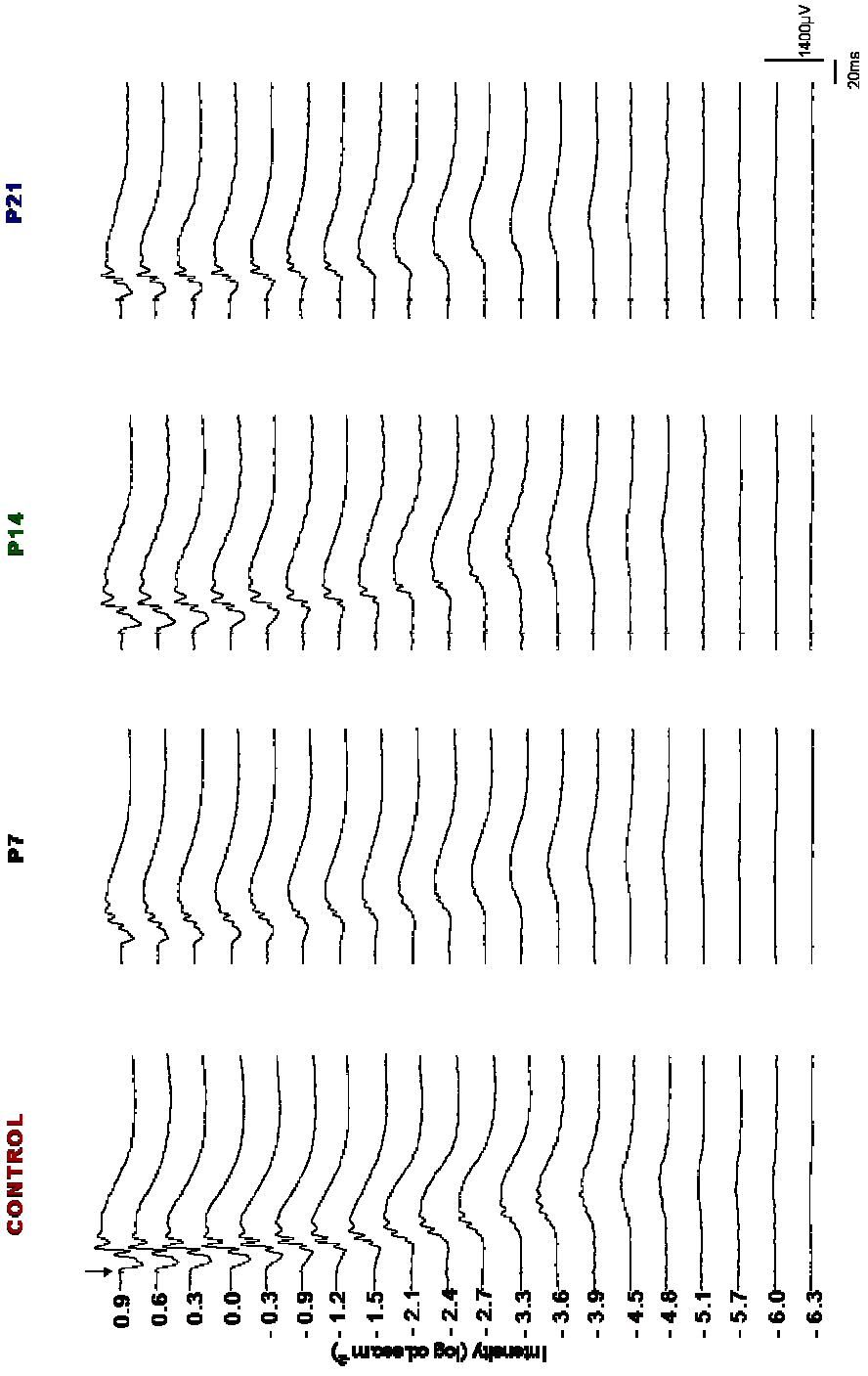

Figure 23: Representative scotopic mixed rod-cone ERG waveforms (P60)

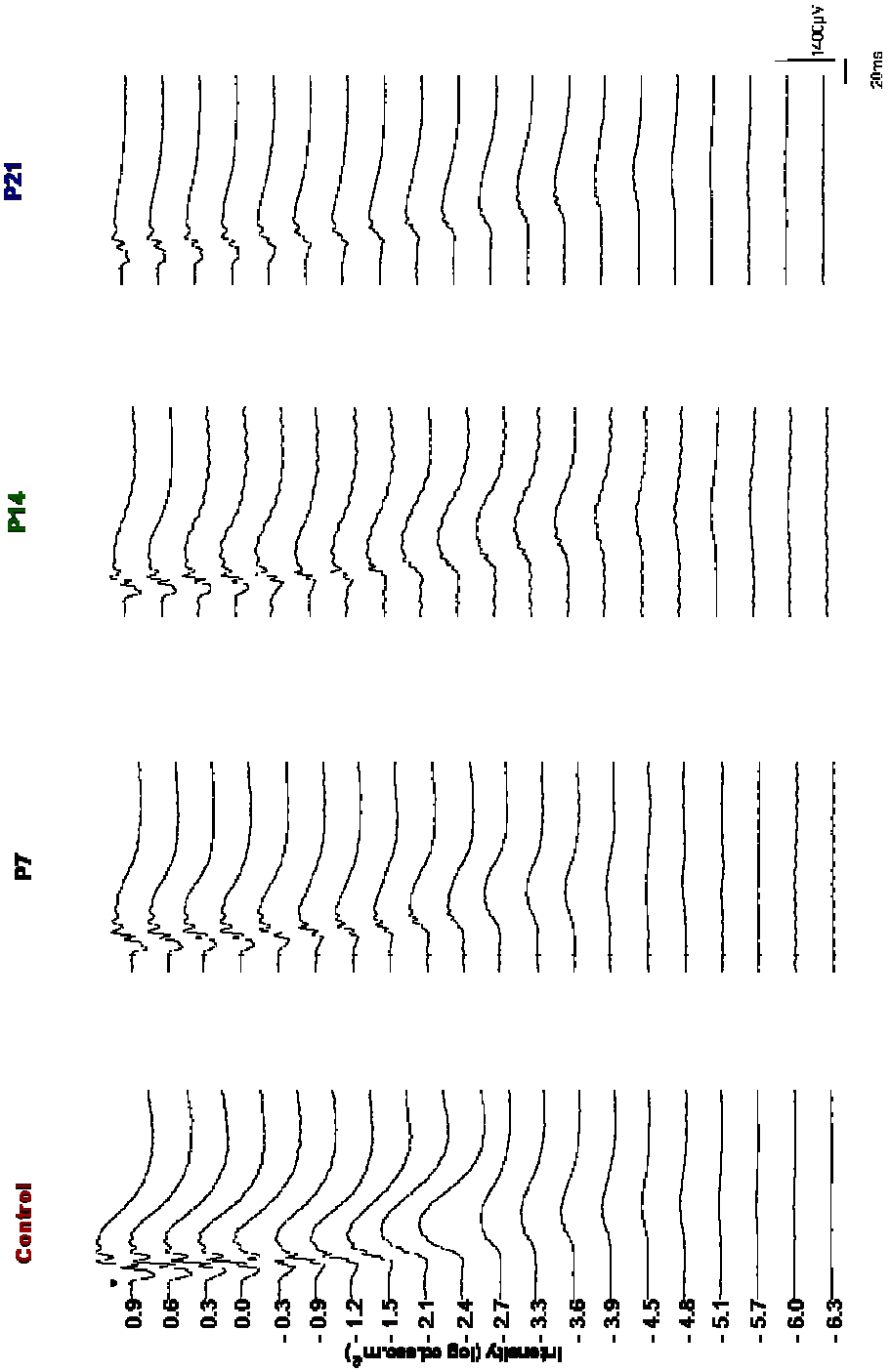

Figure 24: Graphic representation of a-wave (left) and b-wave (right) luminance dose-response curves (P30, P45, P60)

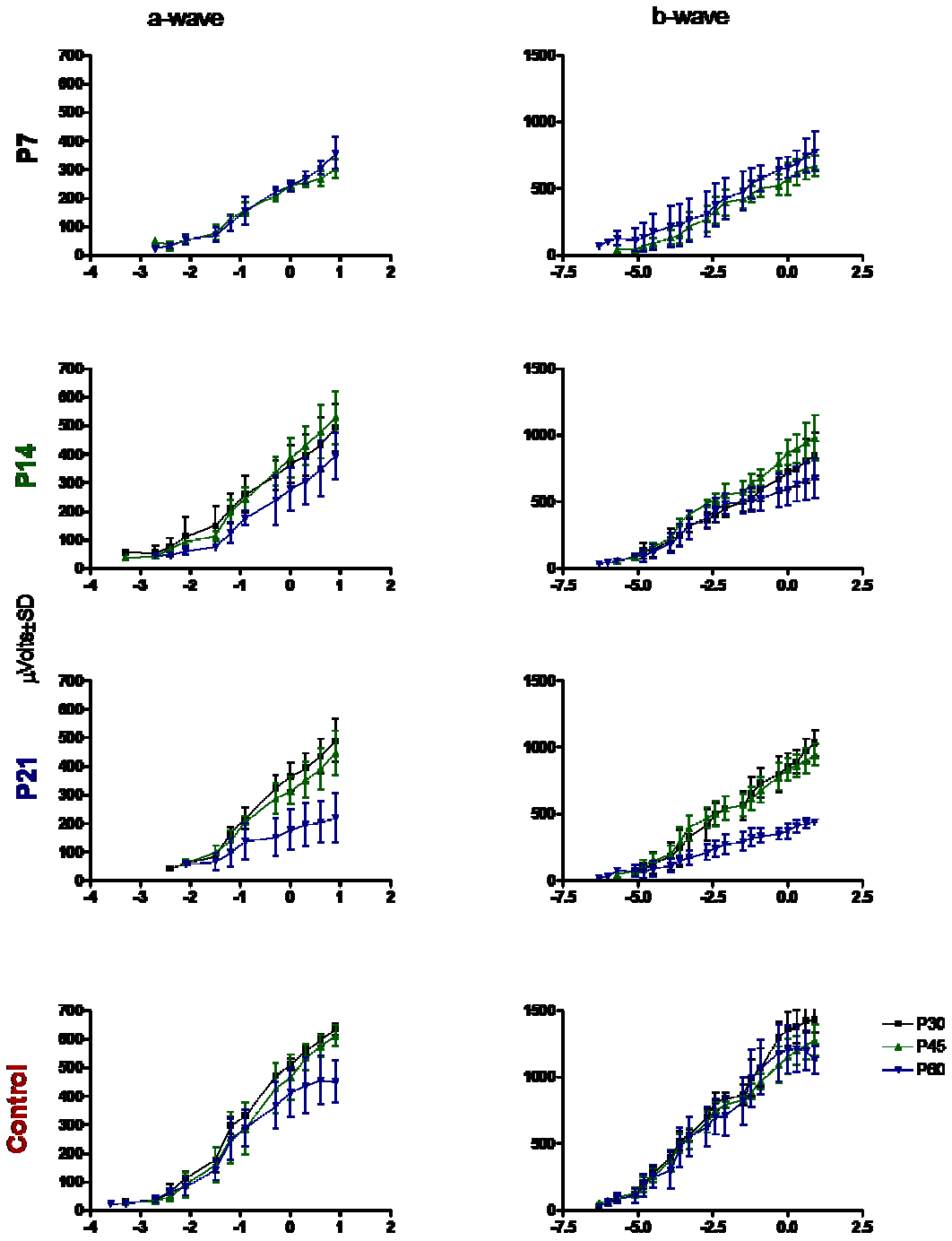

Figure 25: Representative photopic ERG waveforms (top), graphic representation of the mean values of the photopic b-wave amplitudes (bottom) (P30)

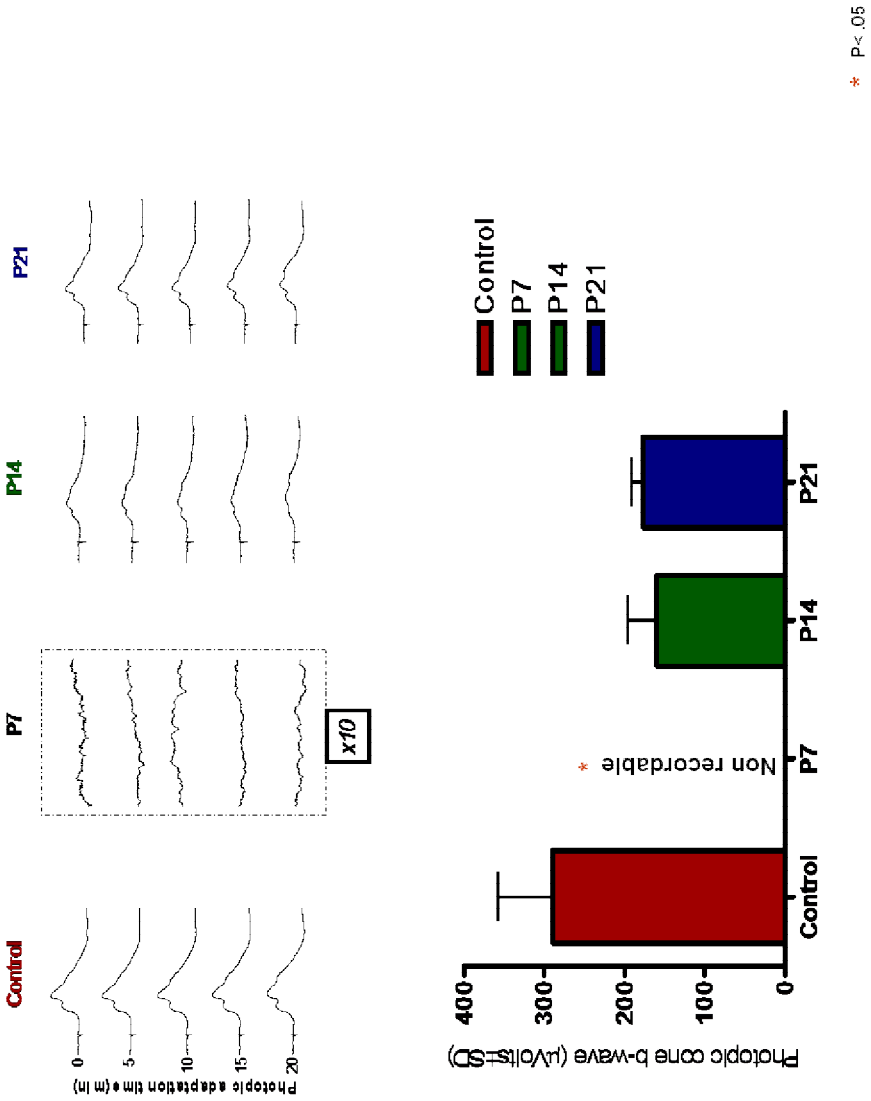

Figure 26: Representative photopic ERG waveforms (top), graphic representation of the mean values of the photopic b-wave amplitudes (bottom) (P45)

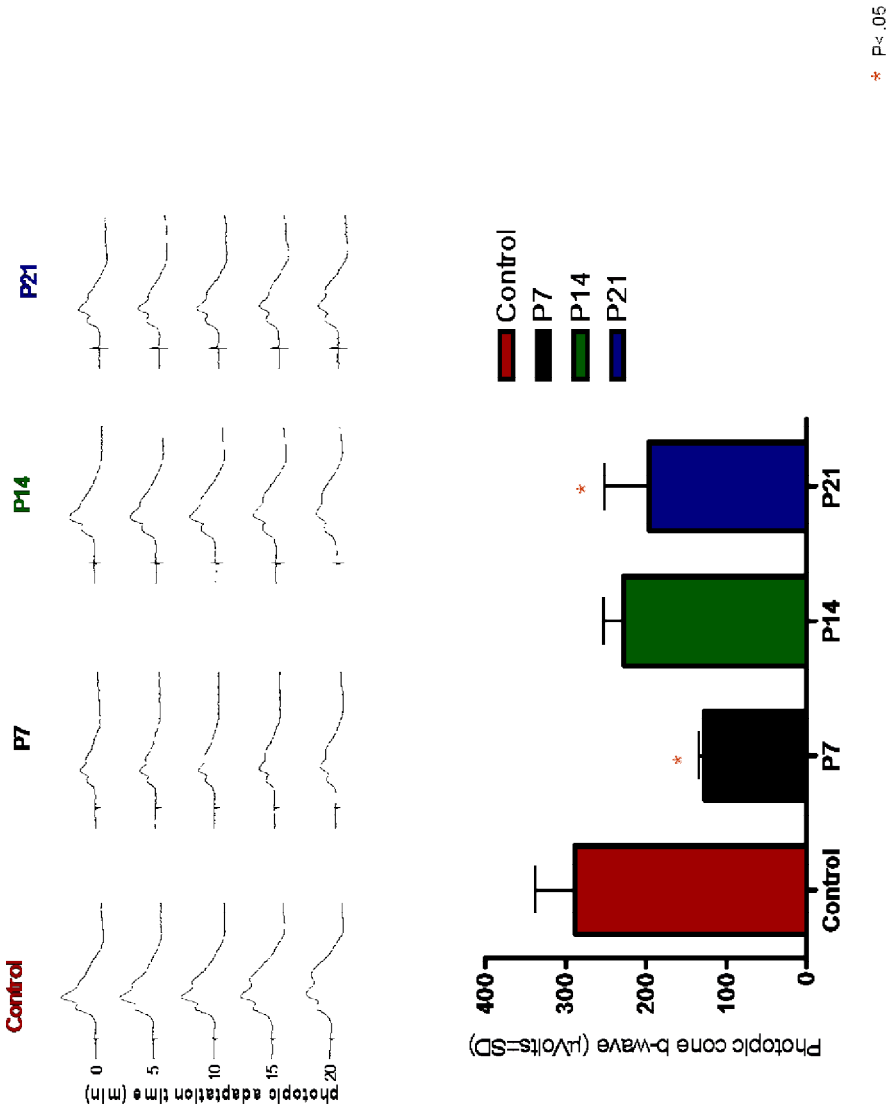

Figure 27: Representative photopic ERG waveforms (top), graphic representation of the mean values of the photopic b-wave amplitudes (bottom) (P60)

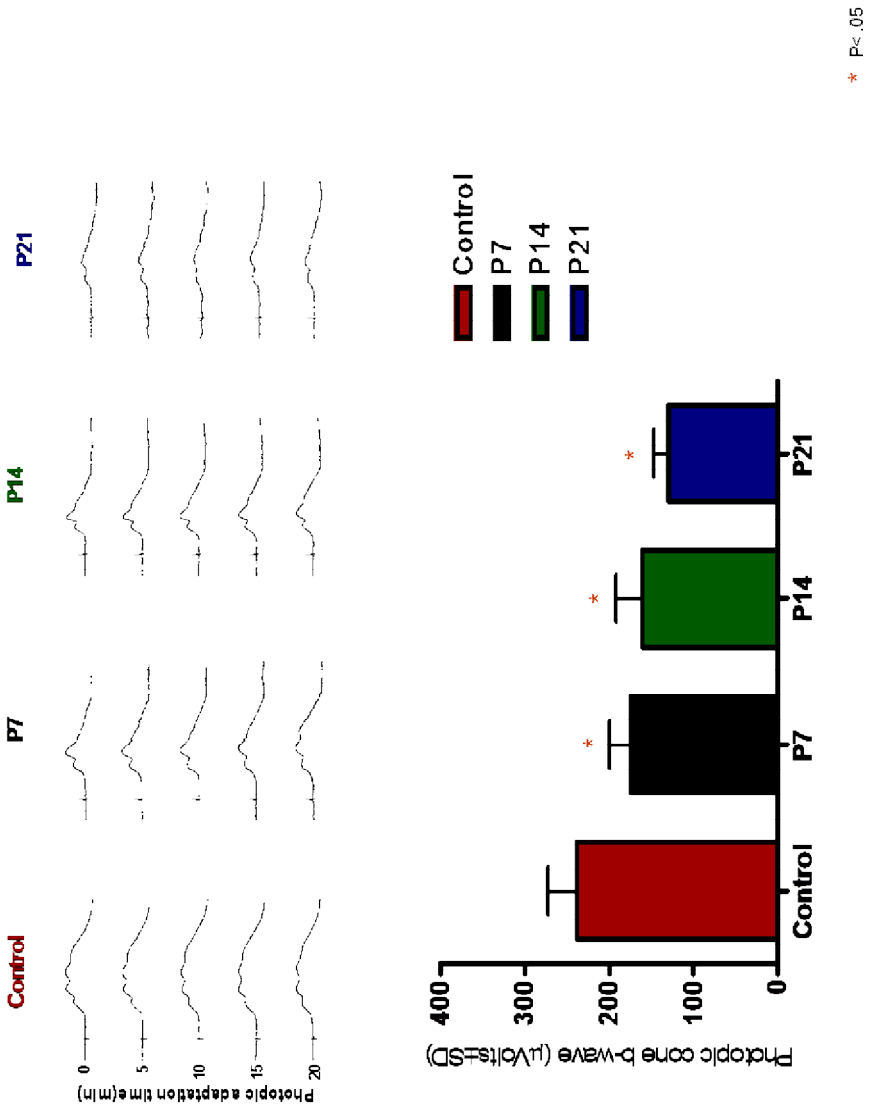

Figure 28: Graphic representation of the mean values of rod Vmax (left) and photopic b-wave (right) amplitudes (P30, P45, P60)

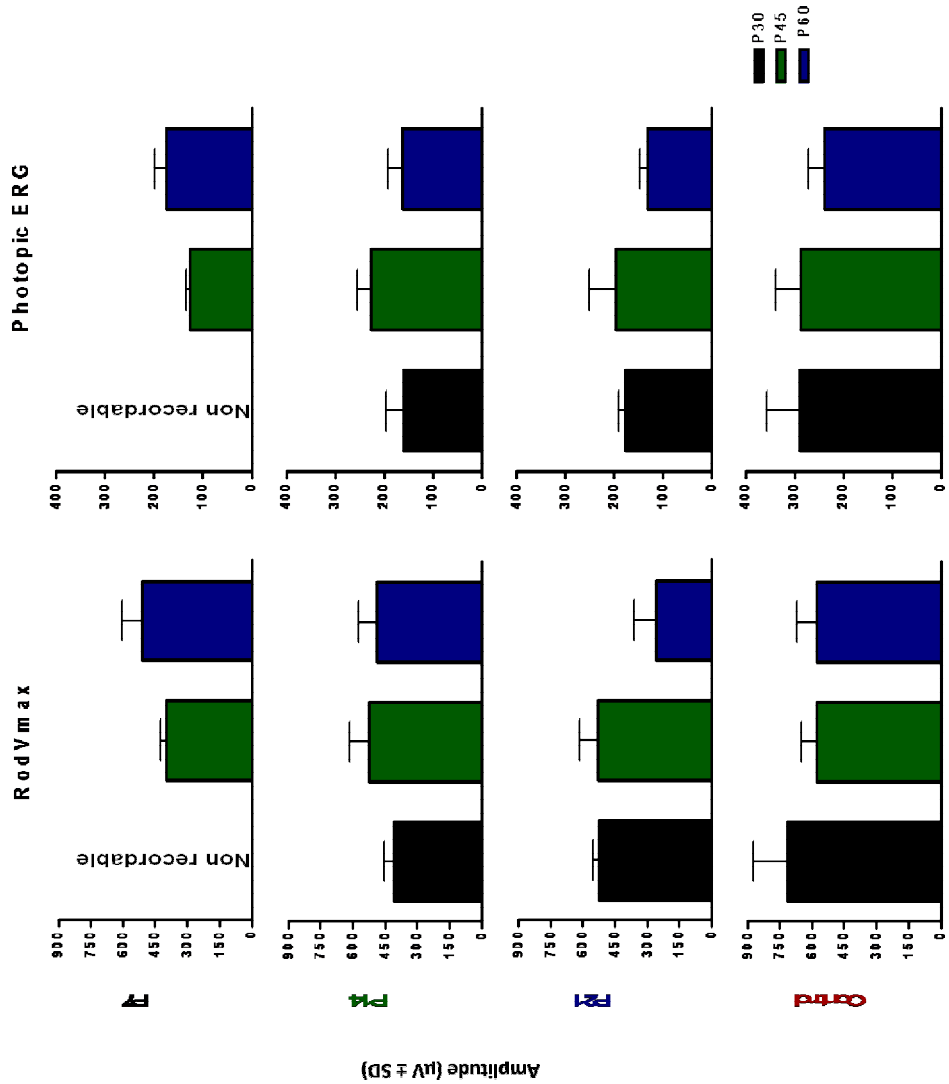

Figure 29: Representative retinal histological sections (left); ONL folding example (right)

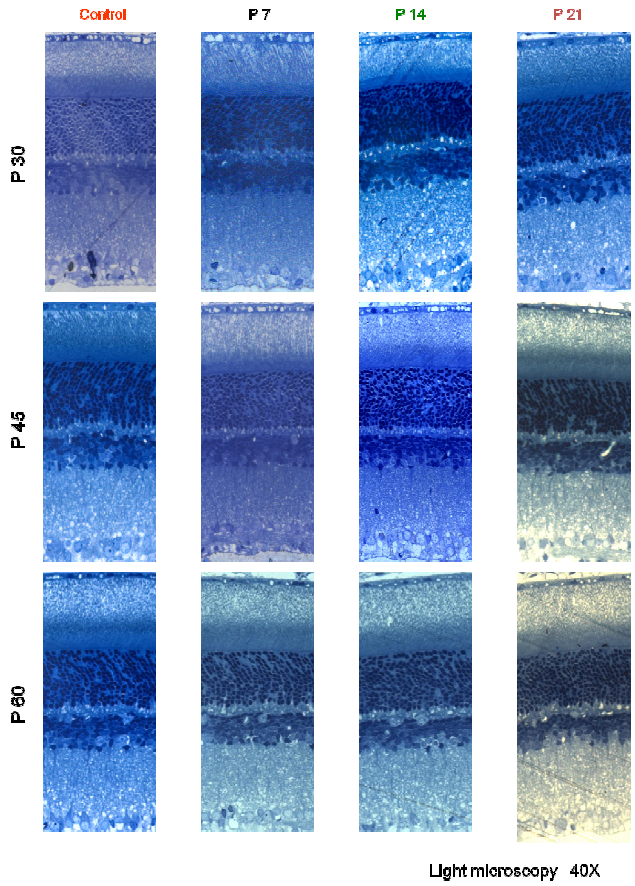

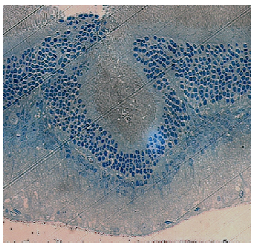

ONL invagination (P60 group at postnatal day P30)

8 TABLES

Table 1: Group data (mean values)

PARAMETERS		NC	DR28
scotopic a-wave	P-30	474.22 ± 81.35 µV	691.26 ± 82.91 µV
	P-60	235.31 ± 35.95 µV	315.66 ± 28.03 µV
scotopic b-wave	P-30	1104.12 ± 134.11 µV	1491.08 ± 39.62 µV
	P-60	626.64 ± 69.56 µV	889.57 ± 23.13 µV
rod V_{max}	P-30	531.76 ± 77.2 µV	764.86 ± 112.02 µV
	P-60	471.63 ± 87.01 µV	536.63 ± 9.70 µV
photopic b-wave	P-30	211.25 ± 36.41 µV	246.01 ± 16.03 µV
	P-60	222.58 ± 41.27 µV	212.19 ± 18.29 µV

Table 2: Group data (mean values)

PARAMETERS		*O_2	DRO_2
scotopic a-wave	**P-30**	287.65 ± 69.38	310.81 ± 24.24 µV
	P-60	214.32 ± 82.09	345.20 ± 17.46 µV
scotopic b-wave	**P-30**	324.79 ± 116.96	616.15 ± 125.43 µV
	P-60	309.18 ± 248.22	504.87 ± 5.36 µV
rod V_{max}	**P-30**	123.15 ± 92.98	306.93 ± 93.26 µV
	P-60	138.08 ± 137.25	280.43 ± 102.25 µV
photopic b-wave	**P-30**	57.18 ± 34.09	109.82 ± 25.14 µV
	P-60	52. 43 ± 44.79	108.79 ± 37.99 µV

*results obtained by Dorfman et al. (2009)

Table 3: Group data (mean values)

Parameters		Control	P7	P14	P21
Scotopic a-wave	P30	633 ± 20	Non recordable	492 ± 82	489 ± 74
	P45	618 ± 34	301 ± 31	527 ±93	445 ± 77
	P60	450 ± 72	356 ± 54	393 ± 80	217 ± 87
Rod-cone b-wave	P30	1428 ± 99	Non recordable	844 ± 171	1029 ± 98
	P45	1273 ±120	666 ± 77	977 ± 168	942 ± 81
	P60	1126 ± 106	773 ± 146	673 ± 149	437 ± 18
Rod Vmax	P30	715 ± 156	Non recordable	408 ± 45	525 ± 28
	P45	578 ± 70	398 ± 28	526 ± 85	529 ± 84
	P60	546 ± 95	509 ± 95	488 ± 83	260 ± 101
Photopic b-wave	P30	290 ± 67	Non recordable	160 ± 34	177 ± 13
	P45	288 ± 49	127 ± 7	227 ± 25	196 ± 55
	P60	238 ± 33	174 ± 25	161 ± 29	130 ± 17

Table 4: Group data (mean values)

Age	Control	P7	P14	P21
P30	51±15µm	48±11µm	49±7µm	48±8µm
P45	43±9µm	42±12µm	42±12µm	41±4µm
P60	39±6µm	38±8µm	39±4µm	38±6µm